

On the stability of the open-string QED neutron and dark matter

Cheuk-Yin Wong^b

¹Physics Division, Oak Ridge National Laboratory^a, Oak Ridge, Tennessee 37831, USA

Abstract We study the stability of a hypothetical QED neutron, which consists of a color-singlet system of two d quarks and a u quark interacting with the QED interaction. As a quark cannot be isolated, the intrinsic motion of the three quarks in the lowest-energy state may lie predominantly in 1+1 dimensions, as in a d - u - d open string. The attractive d - u and u - d QED interactions may overcome the weaker repulsive d - d QED interaction to bind the three quarks together. We examine the QED neutron in a phenomenological three-body problem in 1+1 dimensions with an effective interaction extracted from Schwinger's exact QED solution in 1+1 dimensions. The phenomenological model in a variational calculation yields a stable QED neutron at 44.5 MeV. The analogous QED proton with two u quarks and a d quark has been found to be too repulsive to be stable and does not have a bound or continuum state, onto which the QED neutron can decay via the weak interaction. Consequently, the QED neutron is stable against the weak decay, has a long lifetime, and is in fact a QED dark neutron. It may be produced following the deconfinement-to-confinement phase transition of the quark gluon plasma in high-energy heavy-ion collisions. Because of the long lifetime of the QED dark neutron, self-gravitating assemblies of QED dark neu-

trons or dark antineutrons may be good candidates for a part of the primordial dark matter produced during the phase transition of the quark gluon plasma in the evolution of the early Universe.

Keywords Anomalous soft photons · X17 · E38 · Schwinger QED2 · Open string · Dark matter

1 Introduction

Recent experimental observations of (i) the anomalous soft photons [1, 2, 3, 4, 5, 6, 7, 8, 9], (ii) the X17 particle at about 17 MeV [10, 11, 12], and (iii) the E38 particle at about 38 MeV [13, 14, 15, 16] have generated a great deal of interests [17]-[52]. With a mass in the region of many tens of MeV, the produced anomalous particles appear to lie outside the domain of the Standard Model. Many speculations have been proposed for these objects, including the cold quark-gluon plasma, QED mesons, the fifth force of Nature, the extension of the Standard Model, the QCD axion, dark matter and many others [53].

Among the many proposed explanations for the above three anomalies, the description of the quantized QED mesons [28, 29, 30, 31, 32, 33, 34] has the prospect of linking them together in a consistent framework. We note that the anomalous soft photons are consistently produced as observed excess e^+e^- pairs when hadrons are produced, and they are not produced when hadrons are not produced [1, 2, 3, 4, 5, 6, 7, 8, 9]. The correlated production of anomalous soft photons alongside with hadrons suggests that a parent particle of the anomalous soft photons is likely to contain some elements of the hadrons, such as a light quark-antiquark pair. The transverse momentum range of the anomalous soft photons of many tens of MeV/c suggests further that the parent particle is likely the QED excitation of such a

^aThis manuscript has been authored in part by UT-Battelle, LLC, under contract DE-AC05-00OR22725 with the US Department of Energy (DOE). The US government retains and the publisher, by accepting the article for publication, acknowledges that the US government retains a nonexclusive, paid-up, irrevocable, worldwide license to publish or reproduce the published form of this manuscript, or allow others to do so, for US government purposes. DOE will provide public access to these results of federally sponsored research in accordance with the DOE Public Access Plan (<http://energy.gov/downloads/doe-public-access-plan>), Oak Ridge, Tennessee 37831, USA

^be-mail: wongc@ornl.gov

quark-antiquark pair. For, it was shown by Schwinger previously that massless fermions (and their antiparticles) interacting in a gauge field with a coupling constant g_{2D} in 1+1 dimensions lead to stable bosons with a mass $m = g_{2D}/\sqrt{\pi}$ [54, 55]. A Schwinger boson can be viewed as the stable collective excitation of the fermions and their gauge fields in the vacuum. It can be alternatively viewed as a confined open-string state of a fermion-antifermion pair bound together by their mutual gauge field interaction. We shall review Schwinger's boson in (1+1)D QED in Appendix A and apply it to quarks interacting in QED and QCD in Appendix B. Thus, if we treat the light quarks as Schwinger's massless fermions subject to QED and QCD gauge interactions as discussed in Appendix A and B, the ratio of the mass of a $q\bar{q}$ composite of the QED excitation (a QED meson) to the mass of a $q\bar{q}$ composite of the QCD excitation (a QCD meson) as given by Eq. (B.16) of Appendix B would be of order

$$\frac{m_{\text{QED meson}}}{m_{\text{QCD meson}}} \sim \frac{g^{\text{QED}}}{g^{\text{QCD}}} \sim \sqrt{\frac{\alpha_{\text{QED}}}{\alpha_{\text{QCD}}}} \sim \sqrt{\frac{1/137}{0.6}} \sim \frac{1}{9}, \quad (1)$$

placing the QED meson within the domain of the anomalous soft photons. It was therefore proposed in [28, 29, 30, 31] that QED excitations of quarks may lead to confined, open-string QED mesons with masses of many tens of MeV. These QED mesons may be produced simultaneously along with the QCD mesons when the quark system is excited in high-energy collisions [1, 2, 3, 4, 5, 6, 7, 8, 9], and the excess e^+e^- pairs may arise from the decays of these QED mesons. By examining both the QCD string and the QED string excitations, using the method of bosonization [56, 57, 58, 59, 60, 61, 62, 63, 64, 65] and extrapolating from the QCD string excitations to the QED string excitations, the mass of the $I(J^\pi)=0(0^-)$ isoscalar QED meson was predicted to be 17.9 ± 1.8 MeV and the mass of the isovector ($I(J^\pi)=1(0^-)$, $I_3=0$) QED meson to be 36.4 ± 3.8 MeV [31]. These QED meson masses match those of the X17 particle, the E38 particle, and the possible parent particles of the anomalous soft photons, indicating that these anomalous particles are consistent with their description as QED excitations of the quark vacuum.

It is commonly argued that quarks experience QCD and QED interactions simultaneously and that the quark confinement is a property of quarks in QCD alone. It may appear at first sight that the above suggestion of stable and QED excitations of confining quarks may appear impossible. Is it ever possible for quarks (and antiquarks) to interact with the QED interaction alone without the QCD interaction? Can there be stable collective QED excitations of quarks and antiquarks, similar to the stable collective QCD quark-antiquark excita-

tions? If quarks can interact with the QED interaction alone, can there be additionally other similarly favorable neutral mutiquark systems stabilized by the QED interaction?

With regard to the first question whether it is ever possible for quarks (and antiquarks) to interact with the QED interaction alone, we can consider as an example the production of a quark and an antiquark pair by $e^+ + e^- \rightarrow \gamma^* \rightarrow q + \bar{q}$ or $e^+ + e^- \rightarrow \gamma^* + \gamma^* \rightarrow q + \bar{q}$ with a center-of-mass energy \sqrt{s} in the range $(m_q + m_{\bar{q}}) < \sqrt{s} < m_\pi$, where the sum of the rest masses of the light quark and light antiquark is of order a few MeV and $m_\pi \sim 135$ MeV [66]. The incident $e^+ + e^-$ pair is in a colorless color-singlet state, and thus the produced $q\text{-}\bar{q}$ pair is also a color-singlet pair. The produced $q\text{-}\bar{q}$ pair, if they can ever be produced in this range of \sqrt{s} , can only interact with the QED interaction but not with the QCD interaction, because the QCD interaction would result in a composite $q\text{-}\bar{q}$ hadron state with a center-of-mass energy \sqrt{s} beyond this energy range, in a contradictory manner. It is therefore possible for a quark and an antiquark to interact with QED interaction alone, if they are produced in the range of \sqrt{s} below the pion mass. If the produced quark and the antiquark are not confined by the QED interaction, the produced quark-antiquark pair will appear as a continuum state with separated fractional charges of a quark and an antiquark, at energies away from the bound state energies. The non-observation of fractional charges for the $e^+ + e^- \rightarrow q + \bar{q}$ reaction in this \sqrt{s} range away from the bound state energies, is consistent with the confinement of quarks in QED interactions in (3+1)D.

In other reactions, there are circumstances in which a $q\text{-}\bar{q}$ pair can be produced with a center-of-mass energy \sqrt{s} lower than the pion mass and can interact in the QED interaction alone without the QCD interaction. For example, we mentioned earlier the production of a $q\text{-}\bar{q}$ pair interacting in QED interactions as a possible description for the anomalous soft photons, the X17 particle, and the E38 particle with masses in the range of many tens of MeV, as described in [31]. In other circumstances in the deconfinement-to-confinement phase transition of the quark-gluon plasma in high-energy heavy-ion collisions, a deconfined quarks and a deconfined antiquark in close spatial proximity can coalesce to become a $q\text{-}\bar{q}$ pair with a pair energy below the pion mass, and they can interact in QED interactions alone.

In the dynamics of quarks and antiquarks in a general reaction, the quark currents and the gauge fields are not single-element functions. They are in fact 3×3 color matrices. Quarks in triplet $\mathbf{3}$ representation and

antiquarks in $\mathbf{3}^*$ representation form the product group of $\mathbf{3} \otimes \mathbf{3}^* = \mathbf{1} \oplus \mathbf{8}$, which contains the color-singlet $\mathbf{1}$ subgroup and the color-octet $\mathbf{8}$ subgroup. Quark currents j^μ and gauge fields A^μ in the color-singlet and color-octet subgroups execute collective dynamics within their respective subgroups, as discussed in Appendix A and B. Quarks and antiquarks can therefore interact with the QED interaction alone within the color-singlet subgroup, if their center-of-mass energy is below the pion mass.

To describe the quark-QCD-QED dynamics in detail, we envisage the vacuum to comprise of quarks filling up the negative-energy Dirac sea, with transient quark-antiquark pairs, gluons, and photons lurking here and disappearing there in the space time arena [67, 68]. On top of this vacuum, we introduce initial gauge field disturbances $A_{\text{QED}}^\mu(x)$ and $A_{\text{QCD}}^\mu(x)$ over a space-time region x , which creates valence quarks occupying states above the Dirac sea and valence antiquarks as unoccupied hole states below the Dirac sea. The interaction Lagrangian is [28, 31, 32, 33, 34]

$$\mathcal{L}^{\text{int}} = \mathcal{L}_{\text{QED}}^{\text{int}} + \mathcal{L}_{\text{QCD}}^{\text{int}}, \quad (2)$$

$$\mathcal{L}_{\text{QED}}^{\text{int}} = \sum_{f,a',a} g^{\text{QED}} Q_f^{\text{QED}} \bar{\psi}_{a'}^f \gamma_\mu (A_{\text{QED}}^\mu)_{a'a} \psi_a^f, \quad (3)$$

$$\mathcal{L}_{\text{QCD}}^{\text{int}} = \sum_{f,a',a} g^{\text{QCD}} Q_f^{\text{QCD}} \bar{\psi}_{a'}^f \gamma_\mu (A_{\text{QCD}}^\mu)_{a'a} \psi_a^f, \quad (4)$$

where $\mu = 0, 1, 2, 3$ are the space-time index, $a = 1, 2, 3$ is the color label, f is the flavor label, $g^{\text{QCD}, \text{QED}}$ are the coupling constants, and $Q_f^{\{\text{QED}, \text{QCD}\}}$ is the charge number of f -flavor quark in QED and QCD respectively. In particular, the QED gauge field $A_{\text{QED}}^\mu(x)$ consists of the component $A_0^\mu(x)$ associated with the generator t^0 of the QED U(1) gauge group,

$$A_{\text{QED}}^\mu(x) = A_0^\mu(x) t^0, \quad \text{where } t^0 = \frac{1}{\sqrt{6}} \begin{pmatrix} 1 & 0 & 0 \\ 0 & 1 & 0 \\ 0 & 0 & 1 \end{pmatrix}. \quad (5)$$

The QCD gauge field $A_{\text{QCD}}^\mu(x)$ consists of eight components $A_{1,2,\dots,8}^\mu(x)$ associated with the eight Gell-Mann matrices generators, $t^{1,2,\dots,8}$ of the QCD color SU(3) gauge group,

$$A_{\text{QCD}}^\mu(x) = \sum_{i=1,2,\dots,8} A_i^\mu(x) t^i, \quad 2 \text{Tr}\{t^a t^b\} = \delta^{ab}. \quad (6)$$

The initial QED and QCD gauge field disturbances will act on the quark field through the Dirac equation

$$\gamma_\mu \left[i\partial^\mu + \sum_{i=0}^8 \sum_a g_f^i (A_i^\mu(x) t^i)_{a'a} \right] \psi_a^f(x) = 0 \quad (7)$$

where $g_f^0 = g^{\text{QED}} Q_f^{\text{QED}} = e Q_f^{\text{QED}}$, $g_f^{1,2,3,\dots,8} = g^{\text{QCD}} Q_f^{\text{QCD}}$, $Q_u^{\text{QED}} = 2/3$, $Q_d^{\text{QED}} = -1/3$, and $Q_{\{u,d,s\}}^{\text{QCD}} = 1$. The initial QED and QCD gauge field disturbances will induce a

change of the state vector $\psi_a^f(x)$ of all quark states and subsequently a change of the quark currents $j^{\mu'}(x)$. Just as the gauge fields, the induced quark currents $j^{\mu'}(x)$ are likewise a 3×3 matrices in color space which can be similarly described in terms of 9 independent generators,

$$j^{\mu'}(x) = \sum_{i=0,1,2,\dots,8} j_i^{\mu'}(x) t^i. \quad (8)$$

In particular, they can be divided into the QED quark current $j_{\text{QED}}^{\mu'}(x) = j_0^{\mu'}(x) t^0$ where

$$j_0^{\mu'}(x) = \sum_{f,a',a} g^{\text{QED}} Q_f^{\text{QED}} \bar{\psi}_{a'}^f(x') \gamma^{\mu'}(t^0)_{a'a} \psi_a^f(x) \Big|_{x' \rightarrow x} \quad (9)$$

and the QCD quark currents $j_{\text{QCD}}^{\mu'}(x) = \sum_{i=1,2,\dots,8} j_i^{\mu'}(x) t^i$ where for $i = 1, 2, \dots, 8$,

$$j_i^{\mu'}(x) = \sum_{f,a',a} g^{\text{QCD}} Q_f^{\text{QCD}} \bar{\psi}_{a'}^f(x') \gamma^{\mu'}(t^i)_{a'a} \psi_a^f(x) \Big|_{x' \rightarrow x}. \quad (10)$$

Through the Maxwell equations for QCD and QED, the color-singlet QED current $j_{\text{QED}}^{\mu'}$ will generate a color-singlet QED gauge fields $\tilde{A}_{\text{QED}}^{\mu'}$, while the color-octet QCD currents $j_{\text{QCD}}^{\mu'}$ will generate a color-octet QCD gauge fields $\tilde{A}_{\text{QCD}}^{\mu'}$. Along the evolution loop $A^\mu \rightarrow j^{\mu'} \rightarrow \tilde{A}^{\mu'}$, the requirement that the generated gauge fields $\tilde{A}^{\mu'}$ at the end of loop be the same as the gauge field disturbance A^μ initially introduced provides the condition for stable QED and QCD collective excitations of the quark vacuum as described in Appendix B [28, 31, 32, 33, 34].

For quarks in QCD, the idealization of a flux tube in $(3+1)\text{D}_{\{x^1, x^2, x^3, x^0\}}$ as a one-dimensional string in $(1+1)\text{D}_{\{x^3, x^0\}}$ is well known since the works of the dual resonance model [70], the Nambu-Goto string model [71, 72], the t'Hooft two-dimensional model [86, 73, 74], the inside-outside-cascade model [59], the yo-yo string model [75] and the Lund model [76]. QCD lattice gauge calculations exhibit explicitly the structure of a flux tube in 3+1 dimensions [77, 78, 79].

For quarks in QED, whether quarks are confined in the U(1) QED gauge interaction in (3+1)D has not been unequivocally demonstrated, although there have been strong hints pointing to the confinement of quarks in QED if they can interact in the QED interaction alone. The principal cause of uncertainty arise from the fact that the QED U(1) gauge field admits two different versions of gauge theories with different confinement properties. As emphasized by Polyakov [80, 81] and Drell *et al.* [82], there is the compact U(1) QED gauge theory containing the gauge fields A^μ as angular variables with periodic properties. Defined on a lattice, the compact U(1) QED gauge theory has the gauge field

action [80,81]

$$S = \frac{1}{2g^2} \sum_{x,\alpha\beta} (1 - \cos F_{x,\alpha\beta}), \quad (11)$$

where g is the coupling constant and $F_{x,\alpha\beta}$ is

$$F_{x,\alpha\beta} = A_{x,\alpha} + A_{x+\alpha,\beta} - A_{x+\beta,\alpha} - A_{x,\beta}, \quad (12a)$$

$$\text{with } -\pi \leq A_{x,\alpha} \leq \pi, \quad (12b)$$

which has self-interacting photons. There is also the non-compact U(1) QED gauge field theory with the gauge field action

$$S = \frac{1}{4g^2} \sum_{x,\alpha\beta} F_{x,\alpha\beta}^2, \quad (13a)$$

$$\text{with } -\infty \leq A_{x,\alpha} \leq +\infty, \quad (13b)$$

which has non-interacting photons. Even though the compact and the non-compact theories have the same continuum limit, they have different confinement properties. A pair of opposite charges in non-compact QED interaction are not confined whereas a pair of opposite charges in compact QED interaction are confined under appropriate conditions [80,81,82].

As pointed out by Yang [83], the quantization and the commensurate property of the electric charges of the interacting particles imply the compact property of the underlying QED gauge group. Because quarks are confined and quark electric charges are quantized and commensurate, it is reasonable to propose that quarks and antiquarks interact in the compact QED U(1) interaction. Accordingly, we can apply the results of Polyakov [80,81], Drell *et al.* [82], and Schwinger [54,55] to simplify the dynamics of quarks and the QED gauge field from $(3+1)\text{D}_{\{x^1,x^2,x^3,x^0\}}$ to $(1+1)\text{D}_{\{x^3,x^0\}}$, as is carried out in [34]. Specifically, Polyakov [80,81] showed that a pair of opposite electric charges interacting in compact QED interaction in the transverse $(2+1)\text{D}_{\{x^1,x^2,x^0\}}$ space-time are confined, and that the transverse confinement persists for all non-vanishing coupling constants, no matter how weak. Such a result was subsequently confirmed by Drell and collaborators [82]. As explained in [82], the transverse confinement of the opposite charges in compact QED gauge field in $(2+1)\text{D}_{\{x^1,x^2,x^0\}}$ arises from the periodicity of the gauge field as a function of the spatial angular variable, leading to transverse gauge photons that are self-interacting through a periodic and bounded potential in the neighborhood of the electric charge. These transverse gauge photons interact among themselves, they do not radiate away, and they join the two opposite charges by a confining force [82]. Upon applying Polyakov's result to infer transverse confinement of quarks interacting in compact QED in the transverse space of $\{x^1, x^2\}$, the dynamics in the $(3+1)\text{D}_{\{x^1,x^2,x^3,x^0\}}$ space-time can

be approximated as the dynamics in an idealized $(1+1)\text{D}_{\{x^3,x^0\}}$ space-time, with the information in the transverse degrees of freedom on the $\{x^1, x^2\}$ transverse plane stored as input parameter properties in the idealized $(1+1)\text{D}_{\{x^3,x^0\}}$ space-time. It is necessary to examine in this idealized $(1+1)\text{D}_{\{x^3,x^0\}}$ space-time arena whether quarks and gauge fields are longitudinally confined. If we next consider further that the light quarks can be approximated to be massless, then according to Schwinger's exact solution for massless fermions in such a $(1+1)\text{D}_{\{x^3,x^0\}}$ QED [54,55], a light quark and its antiparticle interacting in the QED interaction will be longitudinally confined just as well and will form a stable QED quark-antiquark system [34].

From such considerations, as reviewed in Appendix A and B and in [28,31,34], we follow Schwinger and we find theoretically that there is a stable QED quark current $j_{\text{QED}}^\mu(x) = j_0^\mu(x)$ which obeys the Klein-Gordon equation with a QED meson mass, $m_{\text{QED meson}}$, in addition to a stable QCD quark current $j_{\text{QCD}}^\mu(x) = j_1^\mu(x)$ along a unit vector in the $t^{1,2,\dots,8}$ generator space which obeys the Klein-Gordon equation with a different QCD meson mass, $m_{\text{QCD meson}}$ [28,31,32,33,34]. In 1+1 dimensional space-time, stable collective dynamics of the QED and QCD currents and their associated gauge fields can be independently excited in their respective color subgroup spaces. The corresponding confined QED and QCD mesons are string-like excitations occurring at different energies in such 1+1 dimensional space-time.

It is interesting to point out that in previous lattice gauge calculations, Wilson, t'Hooft, Polyakov, Kogut, Susskind, Mandelstam, Banks, Jaffe, Peskin, Drell, Guth, Kondo and many others [85,81,86,87,88,89,90,91,82,92,93] showed that fermions and antifermions in the compact QED U(1) gauge interaction in 3+1 dimensions have a confining phase for strong coupling and a non-confining phase for weak coupling. Recent lattice gauge calculations using tensor networks with dynamical fermions for compact QED in 3+1 dimensions confirm such a result [94]. As quarks are fermions, we expect therefore that under appropriate conditions, quarks interacting in QED in 3+1 dimensions can be confined. The observation and the proposed interpretation of the anomalous particles as confined composite $q\bar{q}$ states provide a special impetus to examine in future lattice gauge calculations whether quarks in color SU(3) interacting in compact QED U(1) gauge fields are confined or not, given the quark QED coupling constant and light quark masses as they are and assuming the QCD gauge fields to be non-participating spectators. In this regard, efficient methods of lattice gauge calculations with dynamical quarks using the tensor network [94],

dual presentation [95], magnetic-field digitization [96], regulating magnetic fluctuations [97], or other efficient methods will be of great interest. Clearly, whatever the theoretical predictions there may be, the confining property of quarks interacting in QED interactions in 3+1 dimensions must be tested by experiments. The present investigation on QED mesons and the stable quark systems in QED interactions serves to facilitate the examination of such an important question.

If quarks and antiquarks can interact with the QED interaction alone under appropriate conditions, can there be other similarly favorable neutral quark systems stabilized by the QED interaction between the constituents in the color-singlet subgroup, with the color-octet QCD gauge interaction as a spectator field? Of particular interest is the QED neutron with the d , u , and d quarks. The three quarks form a color product group of $\mathbf{3} \otimes \mathbf{3} \otimes \mathbf{3} = \mathbf{1} \oplus \mathbf{8} \oplus \mathbf{8} \oplus \mathbf{10}$, which contains a color-singlet subgroup $\mathbf{1}$ where the color-singlet current and the color-singlet QED gauge field reside. In the color-singlet system of the three quarks at energies below the QCD nucleon mass, the three quarks can interact with the QED interaction alone. The QED interaction is attractive between quark electric charges of opposite signs, and is repulsive between quark electric charges of the same sign. We depict in Fig. 1 the color-singlet d - u -

tween quark i and quark j , an attractive force for negative $Q_i Q_j$, and a repulsive force for positive $Q_i Q_j$. The attractive d - u and u - d QED interactions between the two d quarks and the center u quark in Fig. 1(a) may overcome the weaker repulsive d - d QED interaction between the two d quarks, to bind the three quarks in the QED neutron. The lowest-energy state is likely to reside in 1+1 dimensions because they are confined, and there is an attraction between the u quark and the d quarks, but a repulsion between the two d quarks. However, the analogous configuration of the QED proton in Fig. 1(b) with two u quarks and one d quark in the u - d - u configuration may likely be unstable because of the stronger repulsion between the two u quarks in comparison with the weaker attractive interaction between the d and the u quarks. We would like to show quantitatively in section 2 that this may indeed be the case. The conclusions we will reach concerning the stability of the QED neutron and proton will also be applicable to the stability of QED antinucleons.

It is worth pointing out that theoretical and experimental investigations on the QED neutron are interesting on many accounts. First is the possibility of its being a new exotic member in the families of particles of the Standard Model. Its properties probably set it apart from other particles because it is a special combination of the light quark fields and the QED gauge fields that has not yet been known up to now. It also calls for a better understanding on the role of the interplay between different fields in the confinement process, whether confinement is limited only to constituents in the presence of the QCD gauge fields, or it suffices to involve also the light quark fields and the QED gauge fields by themselves without the QCD interactions. Clearly, this is a fundamental question that can be answered only by experiments. The observation of the anomalous soft photons, the X17, and the E38 particles indicate that the confined QED meson states can arise from QED interactions of quarks and antiquarks. The investigations presented here and elsewhere [28, 29, 30, 31] will provide additional experimental tests on such a basic property.

There is also the additional interest in the QED neutron, along with the QED mesons and their corresponding antiparticle counterparts, as candidate particles for the primordial dark matter because they are massive, they may be produced during the deconfinement-to-confinement stage of the quark gluon plasma phase transition, and the quark-gluon plasma phase may occur in the early history of the Universe or in high-energy heavy-ion collisions.

To study the stability of the QED neutron and proton with three light quarks, we need to develop the tools for the relativistic three-body problem by cali-

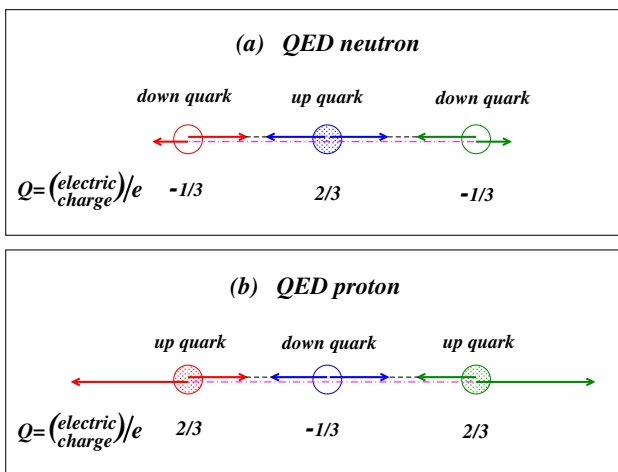


Fig. 1 The schematic picture of a color-singlet three-quark system in 1+1 dimensions in (a) a QED neutron, and (b) a QED proton. The lengths of the arrows represent schematically the forces acting on each of the quarks arising from the QED interactions. The vector sums of the forces acting at each quark show that there are attractive forces binding the d - u - d QED neutron and repulsive forces disrupting the u - d - u QED proton.

d system with three different colors, and we display the different QED forces acting on the three quarks, with the magnitude proportional to $|Q_i Q_j|$ for the force be-

brating the effective two-body QED interaction using Schwinger's exact QED solution for massless fermions in 1+1 dimensions in the Appendix. We generalize the relativistic two-body problem to the three-body problem and evaluate in section 2 the ground state energy for the d - u - d configuration in a variational calculation, which yields a stable QED neutron. Section 3 deals with the property of the lowest state of the QED neutron. We further examine the potential energy as a function of the separations between the quarks. In section 4, we study the stability of the analogous QED u - d - u proton. We find that there is no stable energy minimum for the QED proton. The total potential between quarks interacting in QED alone exhibits repulsive behavior that does not allow the binding of the u - d - u system. In section 5, we discuss other favorable quark configurations for which attractive QED interactions may be present to stabilize the composite multi-quark QED system. In section 6, we examine the decay and the detection of the QED neutron to facilitate its detection. We discuss the implication of the instability of the QED proton and the possibility of the QED neutron to be a dark neutron with a very long lifetime. In Section 7, we conclude our discussions. In Appendix A, we review Schwinger's exact solution of massless fermions in QED in 1+1 dimensions and see how it may be transcribed into a two-body problem. In Appendix B, we study how the color-singlet and the color-octet excitations arise in the quark-QCD-QED medium by applying Schwinger's model to massless quarks in QCD and QED in (1+1)D. In Appendix C we examine the two-body problem from which the effective interaction is determined. Appendix D gives the two-body solution. Appendix E shows that for the lowest energy two-body bound state a variational calculation gives the same result as solving the two-body problem in a wave equation. Appendix F examines the decays and the detection of QED mesons.

2 Stability of the QED neutron with three quarks interacting in QED interactions

To study the QED neutron, we construct a composite system of two d quarks and one u quark by selecting quarks of three different colors to form a color-singlet state and search for its lowest energy bound state. In the formulation of Dirac, Todorov, Crater, Van Alstine, and Sazdjian, and many others [102, 103, 104, 105, 106, 107, 108, 109, 110, 111, 112], relativistic many-body treatments of bound states have been carried out in QCD and QED with a high degree of successes. The basic ingredients consist of treating particles and antiparticles as independent positive-energy entities with effective interactions between them. Each particle obeys

a mass-shell constraint on: (i) the momentum, (ii) the particle mass, and (iii) the effective interactions from the other particles. The effective interactions can be obtained by matching with the perturbative or non-perturbative counterparts of the field theory or by phenomenological considerations. In accordance with Dirac's constraint dynamics [102], the mass-shell constraints must however be compatible with each other, resulting in additional functional requirements or additional terms in the equivalent Schrödinger-type equations whose eigenvalues lead to the eigenstates and the masses of the composite particle in question.

We consider a three-quark system with a two-body effective interaction $\Phi_{ij}(x_{ij})$ arising from the particle j at x_j acting on the particle i at x_i , depending on the relative coordinate $x_{ij} = x_i - x_j$. The lowest-energy state is likely to reside in 1+1 dimensions because quarks are confined, and there is an attraction between the u quark and the d quarks but a repulsion between the two d quarks. We place the d , u , and d quarks on the x -axis with coordinate labels x_1 and x_3 for the two d quarks and x_2 for the u quark. By allowing all x_i coordinates to assume both positive and negative values, while fixing the center of mass position (see Eq. (23) below), we allow all possible arrangement of the ordering of the positions of the three quarks in the variations. We wish to find out quantitatively whether the attractive QED interactions between the d quarks and the u quark can overcome the repulsive and weaker QED interaction between the two d quarks so as to stabilize the QED neutron, as discussed schematically in Fig. 1(a).

For simplicity in our first survey, we neglect particle spins whose effects on the confining effective interaction are expected to be small¹. The spin will lead to a fine-structure splitting of the QED neutron states which can be studied when more data become available. We work in the three-quark center-of-mass system in which $P = p_1 + p_2 + p_3 = (P^0, \mathbf{P}) = (M, 0)$, and the relative coordinate $x_{ij\perp} = (x_i - x_j)$ transverse² to P involves only spatial coordinates x_i and x_j . The three particle momenta in the CM system are

$$p_i = (\epsilon_i, q_i), \quad i = 1, 2, 3, \quad (14)$$

$$\text{where } \epsilon_i = \frac{p_i \cdot P}{\sqrt{P^2}}, \quad q_i = p_i - \frac{p_i \cdot P}{P^2} P, \quad (15)$$

¹Schwinger's exact solution for massless fermions in QED in 1+1 dimensions indicates that the boson mass of the composite fermion-antifermion system depends only on the gauge coupling constant and is independent of the total spin of the fermion-antifermion pair. Consequently, it can be inferred that spin effects on the effective confining interaction are small.

²A space-time vector x_\perp is transverse to another space-time vector P if $x_\perp \cdot P = 0$.

and we consider the particles to be of positive energy only, with $\epsilon_i > 0$. The rest mass M of the composite particle is

$$M = P^0 = \epsilon_1 + \epsilon_2 + \epsilon_3. \quad (16)$$

We generalize the two-body equations of (C.17a) and (C.17b) to the three-body problem by imposing three mass-shell constraints relating the momenta, the masses, and their interactions in the form

$$\mathcal{H}_1|\Psi\rangle = \left\{ p_1^2 - m_1^2 - [\Phi_{12}(x_{12}) + \Phi_{13}(x_{13})] \right\} |\Psi\rangle = 0, \quad (17a)$$

$$\mathcal{H}_2|\Psi\rangle = \left\{ p_2^2 - m_2^2 - [\Phi_{21}(x_{21}) + \Phi_{23}(x_{23})] \right\} |\Psi\rangle = 0, \quad (17b)$$

$$\mathcal{H}_3|\Psi\rangle = \left\{ p_3^2 - m_3^2 - [\Phi_{31}(x_{31}) + \Phi_{32}(x_{32})] \right\} |\Psi\rangle = 0. \quad (17c)$$

The compatibility conditions on the above mass-shell constraints lead to the requirement that $\Phi_{ij}(x_{ij}) = \Phi_{ji}(x_{ij})$ and the variable x_{ij} in the effective interaction $\Phi_{ij}(x_{ij})$ be $x_{ij} = x'_{ij\perp}$, which is transverse to the combined momentum $P_{ij} = p_i + p_j$. This $x'_{ij\perp}$ coordinate should be the relative spatial coordinate in the frame in which the center-of-mass of the system of constituents i and j is at rest. For the three-body problem, the center-of-mass motion of any two constituents i and j has a velocity $V_{ij} = (q_i + q_j) / (\epsilon_i + \epsilon_j)$ and may not be at rest. Even though V_{ij} may not be zero, it will be constrained and limited in a bound state. It is reasonable to neglect such velocities so that we can approximate the $x'_{ij\perp}$ that is transverse to momentum P_{ij} to be the relative coordinate $x_{ij\perp}$ that is transverse to the total center-of-mass momentum P instead. In such an approximation, the relative coordinate $x'_{ij\perp}$ in the effective interaction $\Phi_{ij}(x'_{ij\perp})$ becomes just the relative coordinate $x_{ij\perp}$ of i and j in the three-quark center-of-mass system. Corrections for such an approximation will be of order V_{ij} , which can be taken as velocity-dependent corrections in future refinements.

In the wave equations (17a)-(17c), the phenomenological effective QED interaction extracted from Schwinger's exact QED solution in Eqs. (D.30) and (D.40) in Appendix D is

$$\Phi_{ij}(x_{ij\perp}) = \frac{2\epsilon_i\epsilon_j}{\epsilon_i + \epsilon_j} (-Q_i Q_j) \kappa |x_i - x_j| \text{ with } \kappa = \frac{e^2}{4\pi}, \quad (18)$$

where $e = e_{2D} = g_{2D}^{\text{QED}}$ is the QED coupling constant³ in (1+1)D.

³We adopt here the notations that e is actually e_{2D} , the QED coupling constant in 1+1 dimensions, and e_{4D} is the QED coupling constants in 3+1 dimensions, with the fine structure

Equations (17) and (18) constitute the system of relativistic three-body equations for three quarks interaction in the effective QED interactions. We would like to investigate whether there is a lowest-energy equilibrium state of the QED neutron by using a variational wave function. It is convenient to choose a Gaussian variational wave function of the spatial dimensionless spatial variables y_1, y_2, y_3 with standard deviations σ_1, σ_2 , and σ_3 as variational parameters,

$$\Psi(y_1, y_2, y_3) = N \exp \left\{ -\frac{y_1^2}{4\sigma_1^2} - \frac{y_2^2}{4\sigma_2^2} - \frac{y_3^2}{4\sigma_3^2} \right\}, \quad (19)$$

where $y_i = \sqrt{\kappa} x_i$. The charge numbers of the quarks are $Q_1 = Q_3 = -1/3$, and $Q_2 = 2/3$. The expectation values of (17a)-(17c) using the variational wave function Ψ are

$$\langle \Psi | \frac{\epsilon_1^2}{\kappa} | \Psi \rangle = \langle \Psi | \left\{ \left[\frac{1}{2\sigma_1^2} - \frac{y_1^2}{4\sigma_1^4} \right] + \frac{m_1^2}{\kappa} + \frac{2\epsilon_1\epsilon_2}{\epsilon_1 + \epsilon_2} \left(\frac{2}{9} \right) |y_1 - y_2| + \frac{2\epsilon_1\epsilon_3}{\epsilon_1 + \epsilon_3} \left(\frac{-1}{9} \right) |y_1 - y_3| \right\} | \Psi \rangle, \quad (20a)$$

$$\langle \Psi | \frac{\epsilon_2^2}{\kappa} | \Psi \rangle = \langle \Psi | \left\{ \left[\frac{1}{2\sigma_2^2} - \frac{y_2^2}{4\sigma_2^4} \right] + \frac{m_2^2}{\kappa} + \frac{2\epsilon_2\epsilon_1}{\epsilon_2 + \epsilon_1} \left(\frac{2}{9} \right) |y_2 - y_1| + \frac{2\epsilon_2\epsilon_3}{\epsilon_2 + \epsilon_3} \left(\frac{2}{9} \right) |y_2 - y_3| \right\} | \Psi \rangle, \quad (20b)$$

$$\langle \Psi | \frac{\epsilon_3^2}{\kappa} | \Psi \rangle = \langle \Psi | \left\{ \left[\frac{1}{2\sigma_3^2} - \frac{y_3^2}{4\sigma_3^4} \right] + \frac{m_3^2}{\kappa} + \frac{2\epsilon_3\epsilon_1}{\epsilon_3 + \epsilon_1} \left(\frac{-1}{9} \right) |y_3 - y_1| + \frac{2\epsilon_3\epsilon_2}{\epsilon_3 + \epsilon_2} \left(\frac{2}{9} \right) |y_3 - y_2| \right\} | \Psi \rangle. \quad (20c)$$

Because of the symmetry of the two d quarks we can assume for the lowest-energy state

$$\sigma_1 = \sigma_3, \quad (21)$$

so that the variational parameters consist only of σ_1 and σ_2 . We look for the state with the lowest composite mass M in the variations of σ_1 and σ_2 ,

$$\frac{\delta^2 M(\sigma_1, \sigma_2)}{\delta\sigma_1 \delta\sigma_2} = 0. \quad (22)$$

The motion of the three quarks should maintain a fixed center of mass for the composite system. It is necessary for the coordinates of the three quarks to satisfy the center-of-mass condition on the spatial coordinates,

$$\sum_{i=1}^3 \epsilon_i y_i = 0. \quad (23)$$

The variational wave function Ψ of Eq. (19) is normalized according to

$$\int dy_1 dy_2 dy_3 |\Psi(y_1, y_2, y_3)|^2 \delta(\epsilon_1 y_1 + \epsilon_2 y_2 + \epsilon_3 y_3) = 1. \quad (24)$$

constant defined by $\alpha = \alpha_{4D} = e_{4D}^2 / 4\pi = 1/137$. As pointed out in [84, 28, 69, 34], e_{2D} and e_{4D} are related by the flux tube radius R_T as $e_{2D}^2 = e_{4D}^2 / (\pi R_T^2)$, when the confining flux tube is approximated as an open string without a structure.

Because of the CM condition, there are actually only two independent spatial variables which can be chosen to be y_1 and y_3 . However, we need to treat all three spatial variables as independent in the beginning, and impose the CM constraint (23) only when we evaluate the expectation values in (20) to calculate ϵ_i and M at the end.

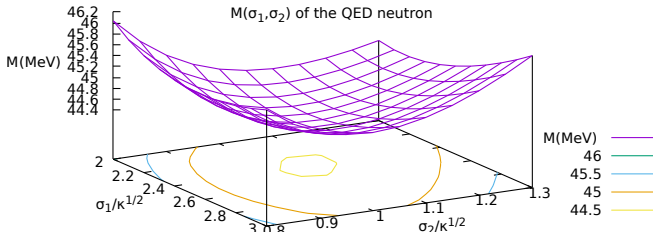


Fig. 2 The mass M of the QED neutron as a function of the variation parameters σ_1, σ_2 in units of $\hbar/\sqrt{\kappa}=8.29$ fm. The QED neutron has an energy minimum at $M = 44.5$ MeV at $\sigma_1/\sqrt{\kappa} = 2.40$ and $\sigma_2/\sqrt{\kappa} = 1.09$.

In the evaluation of the QED neutron mass M , the unknown quantities ϵ_i are needed to define the effective interactions. They can be obtained self-consistently and iteratively with initial guesses. Knowing the effective interactions and the given variational parameters σ_1 and σ_2 , we evaluate the expectation values on the right hand sides of (20a)-(20c) numerically. The calculated values of ϵ_i on the left hand sides of (20a)-(20c) can form the basis of the next iteration until convergence is achieved. In the numerical calculations, we have used quark masses $m_u = 2.16$ MeV and $m_d = 4.67$ MeV [66].

By such variational calculations, we find that the mass M as a function of σ_1 and σ_2 has an energy minimum, $M = 44.5$ MeV, at $\sigma_1 = 2.40\hbar/\sqrt{\kappa}=19.9$ fm and $\sigma_2 = 1.05\hbar/\sqrt{\kappa}=8.71$ fm as shown in Fig. 2.

3 Properties of the lowest-energy QED neutron

Table 1 lists the physical properties of the QED neutron at its energy minimum. The two d quark energies ϵ_1 and ϵ_3 are smaller than the u quark energy ϵ_2 because the two effective interactions in Eq. (20) for each of the d quarks have opposite signs while those for the u quark have the same sign. The root-mean-squared separation between the two d quarks is 28.2 fm and thus the QED neutron spans a length of order many tens of fermi. The wave function of the d quarks have a larger value of the standard deviation σ_1 as compared to the standard

deviation σ_2 of the u quark. In the classical description of an open string [75, 76], the d quarks shuttle about the central u quark in a yo-yo motion back and forth from the left to the right of the u quark and back. When a d quark comes to one side of the u quark, the other d quark goes to the other side to balance the center-of-mass motion. The u quark itself also makes excursions about the geometrical center, as indicated by a smaller value of the standard deviation σ_2 .

Table 1 Properties of the lowest-energy QED neutron

Quantity	Value
M (mass of the QED neutron)	44.5 MeV
$\sqrt{\langle \epsilon_1^2 \rangle} = \sqrt{\langle \epsilon_3^2 \rangle}$ (the d quark)	11.3 MeV
$\sqrt{\langle \epsilon_2^2 \rangle}$ (the u quark)	21.8 MeV
$\sqrt{\langle (x_1 - x_2)^2 \rangle}$ (between d quark and u quark)	20.4 fm
$\sqrt{\langle (x_3 - x_1)^2 \rangle}$ (between two d quarks)	28.2 fm
σ_1 (of wave function for the d quarks)	19.9 fm
σ_2 (of wave function for the u quark)	8.71 fm

The force vectors in Fig. 1(a) give a qualitative description of the various forces leading to the binding of the three quarks in a QED neutron. The variational calculations demonstrate the stability of the QED neutron in a quantitative analysis. It is illuminating to see how the effective interactions between the three quarks can bind them together into a QED neutron from a more quantitative viewpoint as an illustration. For such a purpose, we add the wave equations in (17) and we get the total mass-shell condition

$$\left\{ \sum_{i=1}^3 (\epsilon_i^2 - m_i^2) - \sum_{i=1}^3 \mathbf{q}_i^2 - 2[\Phi_{12}(x_{12}) + \Phi_{13}(x_{13}) + \Phi_{23}(x_{23})] \right\} \Psi(x_1, x_2, x_3) = 0. \quad (25)$$

This is just a three body system with a total effective interaction

$$\Phi_{\text{tot}}(x_1, x_2, x_3) = 2[\Phi_{12}(x_{12}) + \Phi_{13}(x_{13}) + \Phi_{23}(x_{23})]. \quad (26)$$

We can acquire a better understanding how the three quarks can bind together in the QED neutron when we examine various components of the effective interactions between different pairs of quarks as a function of a set of representative spatial coordinates. We can choose a sample set of representative coordinates such that the first d quark coordinate is y_1 , the u quark coordinate is at $y_2=0$, and the second d quark coordinate is at $y_3=-y_1$ because of the CM constraint. For such a sample set of representative coordinates, we can study the behavior of various effective interactions which can be expressed as functions of a single variable y_1 . The various effective interactions $2\Phi_{ij}/\sqrt{\kappa}\epsilon_i$ between quark

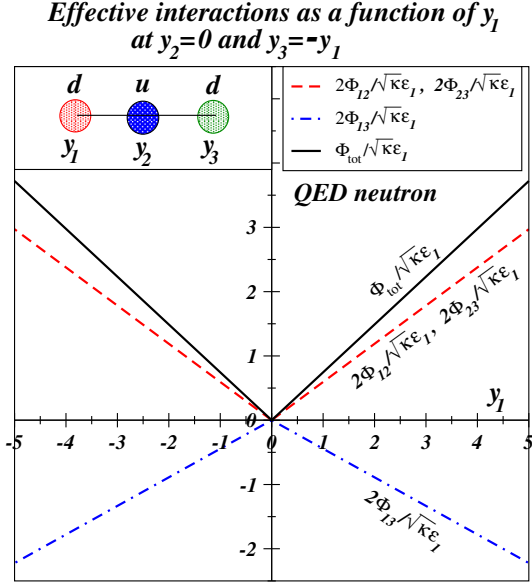


Fig. 3 The effective interaction $2\Phi_{12}$, $2\Phi_{23}$, $2\Phi_{31}$, and $\Phi_{\text{tot}} = 2\Phi_{12} + 2\Phi_{23} + 2\Phi_{31}$ in units of $\sqrt{\kappa\epsilon_1}$ for a QED neutron, where Φ_{ij} is the effective interaction between quarks at y_i and y_j and Φ_{tot} is the total effective interaction, for a selected sample d - u - d arrangement of the three quarks shown at the upper left corner. The potentials are obtained as a function of y_1 , at $y_2 = 0$, $y_3 = -y_1$, where y_1 , y_2 and y_3 are the positions of the d , u , and d quarks respectively,

i at y_i and quark j at y_j and the total Φ_{tot} as a function of y_1 are

$$\begin{aligned} \frac{2\Phi_{12}(y_1, y_2)}{\epsilon_1\sqrt{\kappa}} \Big|_{y_2=0, y_3=-y_1} &= \frac{2\Phi_{23}(x_{23})}{\epsilon_1\sqrt{\kappa}} \Big|_{y_2=0, y_3=-y_1} = \frac{4\epsilon_2/\epsilon_1}{1+\epsilon_2/\epsilon_1} \frac{2}{9}|y_1|, \\ \frac{2\Phi_{13}(y_1, y_3)}{\epsilon_1\sqrt{\kappa}} \Big|_{y_2=0, y_3=-y_1} &= \frac{8\epsilon_3/\epsilon_1}{1+\epsilon_3/\epsilon_1} \left(\frac{-1}{9}\right)|y_1| = \left(\frac{-4}{9}\right)|y_1|, \\ \frac{\Phi_{\text{tot}}(y_1, y_2, y_3)}{\epsilon_1\sqrt{\kappa}} \Big|_{y_2=0, y_3=-y_1} &= \left\{ \frac{8\epsilon_2/\epsilon_1}{1+\epsilon_2/\epsilon_1} \left(\frac{2}{9}\right) + \left(\frac{-4}{9}\right) \right\} |y_1|. \end{aligned}$$

At the minimum energy point, the values of ϵ_1 and ϵ_2 are $\epsilon_1 = 0.4767\sqrt{\kappa}$, $\epsilon_2 = 0.9163\sqrt{\kappa}$, and so $\epsilon_2/\epsilon_1 = 1.922$ and the above dependencies can be evaluated. We show the effective interactions Φ_{tot} and Φ_{ij} between different quarks, as a function of y_1 for the QED neutron at $y_2 = 0$, $y_3 = -y_1$ in Fig. 3. The attractive u - d interactions $2\Phi_{12}/\sqrt{\kappa\epsilon_1}$ and $2\Phi_{23}/\sqrt{\kappa\epsilon_1}$ are shown as the dashed curve. The repulsive d - d interaction $2\Phi_{13}/\sqrt{\kappa\epsilon_1}$ is shown as the dashed-dot curve in Fig. 3. The total effective interaction Φ_{tot} is displayed as the solid curve which is a confining interaction that binds the three quarks together. Hence there is a stable QED neutron arising from the balances of the mutual electrostatic forces between the quarks.

With the above confining potential in Fig. 3 as an illustrative example, we can understand the energy minimum of the QED neutron in two intuitive ways. In the description of the classical string [75, 76], the two

d quarks execute yo-yo motion shuttling about the u quark back and forth after reaching the longitudinal turning points in the confining potential of Fig. 3. In the quantum mechanical description, the attractive net confining QED interaction as shown in Fig. 3 between the quarks is counterbalanced by the quantum stress pressure [113] that arises from the derivatives of the single-particle wave function, reaching the lowest-energy equilibrium between the attractive QED interaction and the quantum stress pressure.

4 The stability of the QED proton and the QED neutron weak decay

We would like to study next whether QED color-singlet proton with two u quarks and a d quark can be stable. For such a calculation, we carry out the variational calculations as in the above QED neutron case, with the u and d quarks in the QED neutron replaced by d and u quarks respectively. That is, we consider the u , d , and u quarks to be placed on the x -axis with coordinate labels x_1 and x_3 for the two u quarks and x_2 for the d quark. By allowing all x_i coordinates to assume both positive and negative values, while fixing the center of mass position (Eq. (23)), we allow all possible arrangement of the ordering of the positions of the three quarks in the variations, including both the linear u - d - u configuration as in Fig. 1(b) and the u - u - d . In this case of QED proton, we have $Q_1 = 2/3$, $Q_2 = -1/3$, and $Q_3 = 2/3$.

Our variations over a very large range of σ_1 and σ_2 values fail to find an energy minimum. Extending the range of σ will only drive the total energy of the system lower with the u quarks farther and farther apart without the energy turning to a minimum. The condition of (22) cannot be satisfied for this case. We can understand the failure by looking at the total potential $2\Phi_{\text{tot}}$ at a sample arrangement shown in Fig. 4. The effective potentials at $y_2 = 0$, $y_3 = -y_1$ for the sample case with $\sigma_1 = \sigma_3 = 2.09\sqrt{\kappa}$ and $\sigma_2 = 2.80\sqrt{\kappa}$, which give $\epsilon_2/\epsilon_1 = 3.71$ are shown in Fig. 4. The magnitude of the sum of the attractive effective interactions $2\Phi_{12} = 2\Phi_{23}$ between the d quark and the two u quarks is smaller than the magnitude of the repulsive interaction $2\Phi_{13}$ between the two u quarks. The total effective interaction Φ_{tot} is repulsive; it decreases as $|y_1|$ increases. Hence, a QED proton does not possess a stable bound state. The QED proton also does not possess a continuum state with isolated quarks because the isolation of quarks as color-triplet quarks is forbidden. Therefore, the QED proton does not exist either as a stable bound state nor a continuum state with isolated quarks. There is no QED proton state.

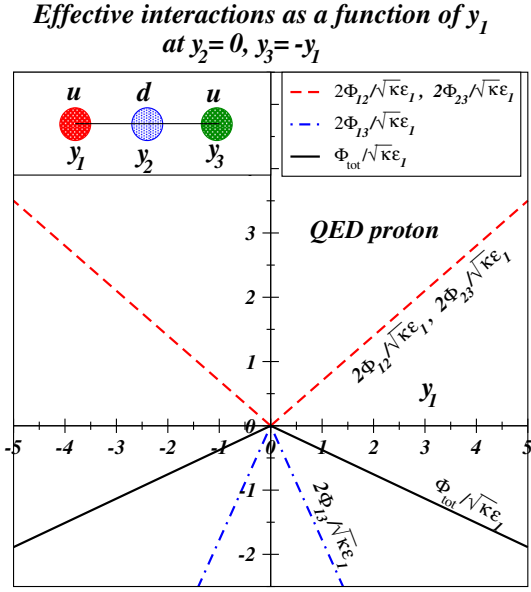


Fig. 4 The effective interaction $2\Phi_{12}$, $2\Phi_{23}$, $2\Phi_{31}$, and $\Phi_{\text{tot}} = 2\Phi_{12} + 2\Phi_{23} + 2\Phi_{31}$ in units of $\sqrt{\kappa\epsilon_1}$ for a QED proton, where Φ_{ij} is the effective interaction between quarks at y_i and y_j and Φ_{tot} is the total effective interaction, for a selected sample u - d - u arrangement of the three quarks shown at the left upper corner. The potentials are obtained as a function of y_1 , at $y_2 = 0, y_3 = -y_1$, where y_1, y_2 and y_3 are the positions of the u, d , and u quarks respectively, The total effective interaction Φ_{tot} shown as the solid curve is a linear repulsive interaction, indicating that the QED proton is not stable.

The absence of a QED proton state has an important consequence on the weak decay of the QED neutron. The weak decay of the QED neutron occurs when a d quark in the three-quark system decays into an u quark. Such a QED neutron weak decay would result in a possible QED proton final state, if a QED proton state could exist. Because there is no final bound or continuum QED proton state for the QED neutron to decay onto, the density of final states for the weak decay of a QED neutron onto a QED proton is zero. Consequently the rate of the QED weak decay into a QED proton is zero. The QED neutron can only decay by a baryon-number non-conserving transition which presumably has a very long life time. Therefore, the lowest energy QED neutron is a stable particle with a very long lifetime and is in fact a dark neutron.

5 Other favorable QED quark configurations and QED quark matter

Although the QED proton with two up quarks and a down quark cannot have a stable bound or continuum state, other neutral QED quark and antiquark systems and their corresponding charge-conjugate counterparts

may have stable configurations arising from quarks and antiquarks interacting in QED interactions in the color-singlet **1** subgroup of the direct product color group, with the QCD gauge interactions as spectator fields. Whether heavy quarks can also interact in QED interactions in this sector cannot be excluded, and it is of interest to examine such a possibility theoretically so as to facilitate future experimental assessments on the occurrence probabilities. By including heavy quarks also among the quarks interacting in QED interactions with the QCD gauge fields as non-participating spectators in Fig. 5, there can be a large number of favorable configurations of neutral open-string systems in which the forces acting on the quarks and antiquarks are subject to a linear QED force that is attractive between two charges of opposite signs and repulsive for two charges of the same sign. The QED attractive forces in these configurations may overwhelm the repulsive forces to lead to stable color-singlet QED composite particles with different flavor contents and quark numbers.

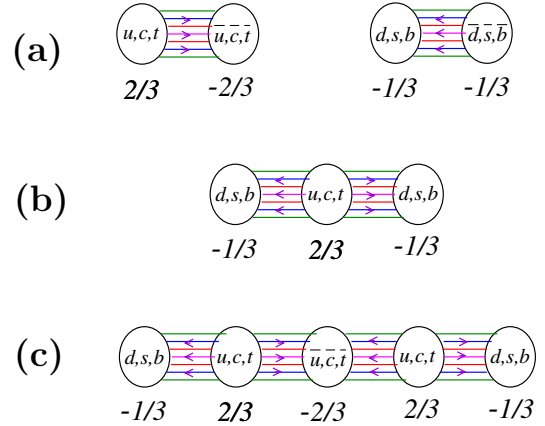


Fig. 5 Some favorable neutral open-string configurations for the lowest energy states involving (a) a quark and an antiquark, (b) three quarks, and (c) three quarks plus a quark-antiquark pair, for quarks and antiquarks interacting in QED forces in the color-singlet **1** subgroup of the product group. Their electric field lines of force are indicated by arrows and the quark electric charge numbers are listed. These open-string configurations may be stabilized by the linear QED forces which are attractive between charges of opposite signs and repulsive between charges of the same sign.

In Fig. 5, we list different choices of flavors for each of the quarks. The quark and the antiquark in Fig. 5(a) have electric charges of opposite signs, and the attractive QED forces between them can stabilize the system. There can be additional flavor mixing considerations if one further assumes flavor $SU(2)$ or $SU(3)$ symmetries as discussed in [31]. Fig. 5(b) shows three quarks, with two quarks of electric charges of $(-1/3)$ and a quark of

charge ($2/3$). They are the analogue of the QED neutron and are likely to be stable. Fig. 5(c) shows a linear chain of five quarks. An example of such a configuration is $d-u-\bar{u}-u-d$ which can be built even longer as $d-u-(u-\bar{u})^n-d$, with $n = 0, 1, 2, \dots$. It has electric charges with alternating signs such that the QED forces between them may be attractive and balanced to stabilize the system.

In the configurations in Fig. 5, one can construct color-singlet states by choosing color-anticolor combinations for the quark-antiquark combinations in Fig. 5(a), three different colors for the three-quark combination in Fig. 5(b), and three different colors for the three-quark combination, and a color and an anticolor for the additional quark-antiquark pair in Fig. 5(c). It will be of interest to study theoretically and experimentally whether these neutral color-singlet quark systems are stable.

Stable QED mesons and QED neutrons, if found to occur, can lead to the QED composite matter, a new type of matter that is a collection of QED mesons and QED neutrons interacting with each other by weak Van der Waal-type interactions between electric multipoles. The QED composite matter can make a transition to become a deconfined quark-QED plasma at the phase transition temperatures $T_{\text{trans}}^{\text{QED}}$. By dimensional analysis following Eq. (??), the ratio of the phase-transition temperatures, $T_{\text{trans}}^{\text{QED}}/T_{\text{trans}}^{\text{QCD}}$, at which QED and QCD mesons become deconfined, would be approximately proportional to their gauge field coupling constants. This places $T_{\text{trans}}^{\text{QED}} \sim T_{\text{trans}}^{\text{QCD}}/10 \sim 20$ MeV. In the finite baryon density regime, the deconfinement phase transition occurs when the degenerate fermion pressure of the dense QED neutrons overwhelms the QED confinement interaction [98]. The quark-QED plasma with varying net baryon densities will have its equilibrium density and its own equation of state. They may be produced in high-energy heavy ion collisions, in the core of neutron stars, or in some stages of neutron star mergers. It has been suggested that the deconfined phase of quark matter may be present in the core of massive neutron stars [114]. In this case, QED quark photon plasma and QED neutrons may also be present in the hadron-quark matter transition region close to the deconfined quark matter core. Future studies on the quark-QED plasma properties and its possible phase transition to QED neutrons will be of great interest.

6 The detection of a QED neutron

A QED neutron is a composite object containing two d quarks and one u quark interacting in QED interactions. The relativistic three-body equations of (17a), (17b), (17c) with a confining potential such as shown

in Fig. 3 are expected to have many eigenstates and eigenvalues. The inclusion of spin-spin, spin-orbit, and other interactions between the quarks in a future fully three-dimensional calculation will add a greater degree of complexity to the spectrum of the QED neutron.

As the detection of a QED neutron will depend on its decay products, we would like to examine how a QED neutron decays from an excited state n_{QED}^* (initial) to a final state n'_{QED} (final). We note first of all what it will not do. It will not dissociate itself into isolated quark constituents because of the non-isolation nature of the quarks. It will not decay by weak interactions into a positively charged entity because there is no bound or continuum final QED proton state.

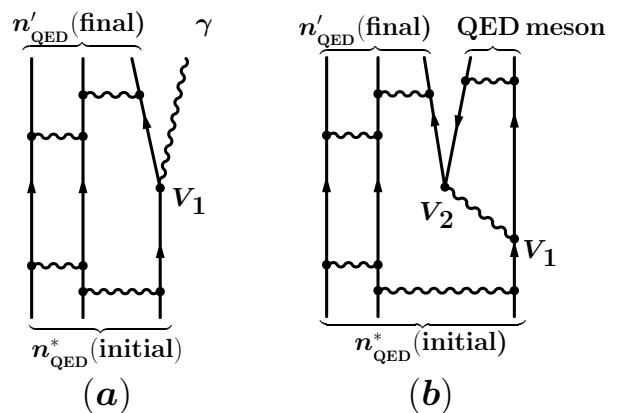


Fig. 6 The decay modes of a QED neutron from an excited eigenstate n_{QED}^* (initial) to the final eigenstate n'_{QED} (final): (a) by the emission of a photon, and (b) by the emission of a QED meson which subsequently can decay into real or virtual photons, or a dilepton pair as described in Fig. 9(a), 9(b), and 9(c) in Appendix F.

In 1+1 dimensions, an excited state of QED neutron cannot decay as the photon is represented in effect by an effective potential Φ as discussed in Appendix C, and the quarks do not radiate photon. In the physical 3+1 dimensions, the transverse structure of the flux tube must be taken into account and the photon emission channel from the quark opens up. A quark can make a sharp change of its trajectory turning to the transverse direction with the emission of a photon from the excited n_{QED}^* . By such an emission process at the vertex V_1 as depicted in diagrams in Fig. 6(a), a quark in an excited QED neutron at the initial excited eigenstate n_{QED}^* (initial) can de-excite to reach the final eigenstate n'_{QED} (final). The multipolarity of the photon transition will depend on the spins and the parities of the initial and final states in question. Alternatively, a valence quark in an initial excited eigenstate n_{QED}^* (initial) can de-excite by the emission of a photon at the vertex V_1 in Fig. 6(b) leading to the production of a quark-

antiquark pair at the vertex V_2 . The produced quark can join up with the remaining two quarks of the initial QED neutron n_{QED}^* (initial) to become the final QED neutron eigenstate n'_{QED} (final), while the produced antiquark can combine with the valence quark to form a QED meson. In such a decay with the emission of a QED meson as depicted in Fig. 6(b), the flavor of the produced pair at V_2 must agree with the flavor of the valence quark emitting the virtual photon at V_1 so that the flavor and the charge of the final QED neutron remains unchanged.

It is easy to envisage that successive emissions of photons and QED mesons will allow an excited QED neutron n_{QED}^* to de-excite, and eventually to reach the lowest energy QED neutron state. Through out the de-excitation process, the three quarks constituents remain bound to each other as an entity, in the conservation of the QED neutron number, while the emitted QED mesons will decay into real photons, virtual photons in the form of dileptons, or a dilepton pair as described by diagrams Figs. 9(a), 9(b), and 9(c) in Appendix F. At the end of the de-excitation, only the ground state QED neutron remains and it does not radiate because it is the lowest energy QED neutron state. Because the lowest-energy QED neutron ground state does not decay or radiate, it is therefore a QED dark neutron.

With the exception of the QED dark neutron which has no decay products, the detection of a QED neutron can be carried out by searching for their decay products of photons and QED mesons arising from the de-excitation of the excited QED neutron states with the emitted QED mesons detected as diphoton resonances. We envisage that by the coalescence of the quarks of different colors, QED neutrons at the lowest-energy state as well as the excited states may be produced during the deconfinement-to-confinement phase transition of the quark gluon plasma. The de-excitation of the excited QED neutron states will yield photons and QED mesons of various energies exhibiting the spectrum of the QED neutron system. The de-excitation energies provide information on the QED neutron structure. We may rely on the presence of these emitted photons and QED mesons to reconstruct the complete spectrum of the QED neutron. The de-excitation may also go through many steps with sequential emissions of QED mesons and/or photons. Accordingly, we can look for unknown photons and QED mesons that accompany the production of other photons and QED mesons.

We note with keen interest that QED neutrons may be produced by the coalescence of deconfined quarks in the core of a dense neutron star or in high-energy heavy-ion collisions during the phase transition of the quark gluon plasma. The production of the QED neu-

tron or its excited states can be used as a signature for the quark-gluon plasma production, if the QED neutron can be so identified. It is necessary to identify the QED neutron if it is produced. A QED neutron can be identified by its QED meson emission spectral lines which exhibit its own characteristic structure. With the mass of the lowest energy QED neutron state predicted to be 44.5 MeV, and if a harmonic oscillator spectrum for the QED neutron can be an order-of magnitude guide, we expect the masses of the emitted QED mesons in the decay of an excited QED neutron state to be of order 50 MeV. We can therefore estimate the production of diphoton resonances with an invariant mass of order 50 MeV to accompany the production of the QED neutron. A way to distinguish those QED mesons as arising from the QED neutron decay or from a $q\bar{q}$ pair production is to study the differences of the QED meson emission spectral lines as a function of the probability for the occurrence of deconfinement, which is correlated with the mass, energy, and centrality of the high-energy collision process. For those collisions with a low probability leading to deconfinement, the detected QED mesons emission spectral lines will not contain those lines emitted from the excited QED neutrons. On the other hand, for collisions with a high likelihood of attaining deconfinement, there will be excited QED neutrons with the accompaniment of the emission of QED mesons with these spectral lines from their de-excitation. By judicial correlations with the probability of such collisions, those QED meson spectral lines associated with the de-excitation of the excited QED neutrons may be separated. The on-set of these extra QED meson lines arising from the decay of excited QED neutrons may be a good signature of the on-set of deconfinement and a signature of the quark-gluon plasma formation.

The search of the QED neutron may also be carried out by elastic and inelastic collisions of the QED neutron with electrons in semiconductors and superconductors, using detectors designed to search for dark matter particles with a mass below 1 GeV/ c^2 . (See Ref. [115] for a review and a list of references for such detectors). The proposed QED neutron has a predicted mass of 44.5 MeV. It is a linear electric quadrupole and it interacts with an electron by the electromagnetic quadrupole interaction $e^2 a^2 \cos^2 \theta / 3 |\mathbf{r}|^3$ where \mathbf{r} is the radius vector from the center of mass of the QED neutron to the electron, θ is the opening angle between \mathbf{r} and the QED neutron linear axis, and a is the separation between the u and the d quark. The separation a has been estimated in Table I to be 20.4 fm. In a charged-coupled device (CCD) detector, the collision between the QED neutron and the electrons of the device may promote an electron from the valence band to

the conduction band. In a transition-edge sensor (TES) detector, which is a superconducting thin film held very close to its transition temperature, the collision may deposit energy onto the thin film. As a result of the energy deposition, the superconducting film will make a transition to the normal state signaled by an increase in its resistance. Another method makes use of a superconducting nanowire single-photon detector (SNSPD) of a thin film of superconducting material carrying a constant applied current. The collision between the QED neutron and the electrons of the detector may disrupt the superconductivity and create a measurable signal. Future studies of the feasibility on the search for the QED neutron using semiconductor and superconductor devices will be of great interest.

7 Summary, Conclusions, and discussions

The recent observations of the anomalous soft photons, the X17 particle, and the E38 particle have been consistently interpreted as the production of QED mesons in [28, 29, 30, 31] arising from the QED excitation of quarks and antiquarks in the QCD+QED gauge field vacuum. Heretofore our usual experience of quarks interacting with gauge fields have been confined mainly to the situation with quarks interacting with both QCD and QED gauge interactions simultaneously, and they are invariably accompanied by gluon exchange interactions. How is it possible for a quark and an antiquark to interact with the QED interaction alone without the QCD interaction?

We have presented arguments in the Introduction to show that a quark and an antiquark can interact with the QED interaction alone if they are produced in the range $(m_q + m_{\bar{q}}) < \sqrt{s} < m_\pi$. We note that the QED and QCD excitations of the quark vacuum can be independent excitations. The important ingredient in resolving the conceptual difficulties rests on the fact that the quark currents and gauge fields are not single-element quantities in QED and QCD dynamics. On the contrary, they are 3×3 matrices in color space, forming a color-singlet **1** subgroup and a color-octet **8** subgroup. The quark QCD and QED currents and gauge fields can be independently excited in their respective subgroups. Hence, there can be QED excitations at the lower energies of many tens of MeV, leading to the production of the QED mesons, with the QCD gauge fields as non-participating background spectators.

If light quarks can interact with QED interactions in the color-singlet sector with the QCD interaction as non-participating background fields, a new frontier will be opened up for exploration because quarks carry electric charges, electric charges of opposite signs attract,

and attractive interactions result in stable and confined composite quark states. There will be many composite systems of light quarks and antiquarks in which the attractive QED forces allow the composite system to form bound and confined states. The many quantum numbers that characterize the quarks will also add complexities to the spectrum of these composite particles. For example, for light quarks with two flavors and $S=0$ moving in phase and out of phases with each other, we show earlier that there can be the $(I=0, I_3=0)$ state at 17.9 ± 1.8 MeV and the $(I=1, I_3=0)$ state at 36.4 ± 3.8 MeV. We do not know whether QED mesons formed by a light quark and a light antiquark of the same flavor are allowed or not. If they are allowed, then by using the semi-empirical formula for the QED meson state energy developed in [31], one locates theoretically the $S=0$ single-flavor excitation $d\bar{d}$ QED meson state at 21.2 ± 2.1 MeV and the $u\bar{u}$ QED meson state at 34.7 ± 3.5 MeV.

The possible occurrence of the QED mesons can be tested by searching for the decay products of two real photons, two virtual photons in the form of double dilepton pairs, or a single dilepton pair. The X17 particle observed in the decays of the ${}^4\text{He}^*$ and ${}^8\text{Be}^*$ [10, 11] with an e^+e^- invariant mass of 17 MeV and the state at 19 ± 1 MeV in emulsion studies [12] match the predicted mass of the isoscalar $0(0^-)$ QED meson [31]. The E38 MeV particle, observed in high-energy $p\text{C}$, $d\text{C}$, $d\text{Cu}$ collisions at Dubna [13, 14] with a $\gamma\gamma$ invariant mass of about 38 MeV, matches the predicted mass of the isovector QED meson [31]. These are encouraging experimental observations. The QED ($u\bar{u}$) and QED ($d\bar{d}$) states have yet to be located and identified experimentally. Further experimental measurements in the low invariant mass region will be of great interest.

The QED mesons are not the only color-singlet composite states arising from quarks interacting in QED interactions in the color-singlet subgroup, with the QCD gauge fields as non-participating spectators. The QED neutron with two d quarks and one u quark with three different colors can form a color-singlet composite system. The QED neutron can be stable because the attractive QED interactions between two d quarks and the u quark overcome the weaker repulsion between the two d quarks. With a phenomenological three-body model in 1+1 dimensions with an effective interaction between electric charges extracted from Schwinger's exact QED solution, we find quantitatively in a variational calculation that there is a QED neutron energy minimum at a mass of 44.5 MeV. The analogous QED proton with two u quarks and a d quark has been found to be too repulsive to be stable and does not have a bound or continuum state.

Because of its composite nature, there will likely be many excited states in the QED neutron. The excited states are expected to decay by emitting photons and/or QED mesons to make transitions to lower QED neutron states. One of the two d quarks may decay into an u quark by way of the weak interaction. However, because the QED proton does not possess a stable bound state nor a continuum state of isolated quarks, the rate of the QED neutron weak decay into a QED proton is zero.

Among all QED neutron states, the ground QED neutron state located at 44.5 MeV distinguishes itself from higher excited QED neutron states as a stable particle without decay products. It can only decay by a baryon-number non-conserving transition, which presumably has a very long lifetime. As a consequence, the lowest state QED neutron is a dark neutron. The QED antineutron ground states is likewise a dark antineutron. The only mode of destruction for a QED dark neutron and a QED dark antineutron is their mutual annihilation, with the production of photons and QED mesons.

It is of interest to discuss the relation between the QED neutron at 44.5 MeV and the QCD neutron at 939.6 MeV that is confined by QCD gauge interactions. We envisage that the QED neutron is an energy minimum in the color-singlet subgroup of quark current and QED gauge field, while the QCD neutron is an energy minimum in the color-octet subgroup of quarks interacting with the exchanges of gluons between quarks. They are similar to the multiple energy minima which occur in the collective energy surface of nuclear systems in [116,117]. As members of different subgroups, they do not mix in the lowest order but can be mixed in second-order perturbation theory by photon interactions. The mixing of QCD neutron in the QED neutron may be small because the QED neutron can be connected to the QCD neutron by electromagnetic interactions but the difference in their longitudinal extensions of wave functions and the large energy denominator in second-order perturbation theory may make the mixing quite small. The sea quarks arise predominantly from the splitting of the gluons into quark-antiquark pairs which appear in the color-octet subgroup of the product group. Because the QED neutron resides in the color-singlet subgroup, the presence of the sea quarks [67,68] in the QCD color-octet subgroup will not likely affect the stability of the QED neutron.

On account of their being predicted to be stable particles with a very long lifetime without decay products, the QED dark neutrons and QED dark antineutrons may be good candidate particles for a part of the dark matter. We envisage that in the early evolution of

the Universe after the big bang, the Universe will go through the quark-gluon plasma phase with deconfined quarks and gluons. As the primordial matter expands and cools down the quark-gluon plasma undergoes a phase transition from the deconfined phase to the confined phase, deconfined quarks of three different colors may coalesce to form color-singlet states. While many of the color-singlet systems of three quarks have sufficient energy to form hadrons, there may be some produced color-singlet three-quark systems in which their total energy is below the QCD neutron energy of about 1 GeV. These three-quark systems may form QED neutron states that are bound by QED interactions. The de-excitation of the excited QED neutron state will find its way down to the lowest energy state of the QED dark neutron. Such QED dark neutrons and its excited states may occur at the deconfinement-to-confinement phase transition of the quark-gluon plasma and may be a signature of the deconfinement-to-confinement transition of the quark gluon plasma in high-energy heavy-ion collisions. Self-gravitating assemblies of QED dark neutrons may be stable astrophysical objects. Because of its long lifetime, self-gravitating QED dark neutron assemblies (and similarly QED dark antineutron assemblies) of various sizes may be good candidates for a part of the primordial dark matter produced during the deconfinement-to-confinement phase transition of the quark gluon plasma in the evolution of the early Universe.

In another matter, LIGO recently observed the merger of two neutron stars through the detection of their gravitational waves in 2017 [118]. Such a merger will likely lead to the production of a quark matter with deconfined quarks [119,120,121]. The authors of [119,120] proposed a new signature for a first-order hadron-quark phase transition in merging neutron stars, which may provide the opportunity to study the properties of the post-merger quark matter. As the quark matter cools and undergoes the deconfinement-to-confinement phase transition during the merging process, the coalescence of deconfined quarks to become confined quarks will produce QED neutrons in the post-merger environment.

In another astrophysical frontier, it has been suggested that deconfined quark matter may be present in the core of a massive neutron star [114]. In such a neutron star, the transition region close to the core may contain QED neutron matter arising from the coalescence of deconfined quarks. In matter of modeling massive neutron star mergers of such a type, it may be necessary to take into account the presence of such a QED neutron region. Therefore, the study of the equation of states and the thermodynamical and phase transition properties of the QED neutron matter will be of

great interest. QED neutrons in the neutron star environment will experience a strong magnetic field which will affect the QED neutron in a significant way. While the confinement of QED neutron may continue to be operative, we expect that the additional magnetic interaction will set the QED neutron into a rotational motion so that the quarks in the QED neutron will go from a 1+1 dimensional dynamics to a full three-dimensional dynamics. It will be of interest to study how the magnetic field will affect the QED neutron and its stability.

As it is suggested here that the confinement to deconfinement phase transition at the early history of the Universe in the quark-gluon plasma phase may generate the QED dark neutron assemblies as seeds for the primordial dark matter, it will be of great interest to study whether QED dark neutrons and/or its excited states may be produced in high-energy heavy-ion collisions where quark gluon plasma may be produced. The detection of the QED dark neutrons may be made by searching for the photons and/or QED mesons during the de-excitation from its excited states. The de-excitation of the excited QED neutron states will yield photons and QED mesons with its own characteristic QED meson emission spectrum. The capability of precise dilepton measurements in high-energy heavy-ion collisions may make it possible to study the spectrum of the produced QED mesons through their decays into two virtual photons, as discussed in Appendix F. We may rely on the presence of these emitted photons or produced QED mesons to reconstruct the spectrum of the QED neutron.

For simplicity in the present first survey of the QED neutron, we have neglected the spin degree of freedom. While the spin will not likely affect the stability, the quark confinement, and the gross structure of the QED neutron, it will play a significant role in the fine structure and the spectrum of the QED neutron. The spin degree of freedom, along with the orbital angular momentum, the collective rotation, and the collective vibration should be taken into account in future studies. Theoretical investigations on the internal structure and the energy spectrum of the QED neutron will be valuable to assist the detection of the produced QED neutrons. How the QED mesons and QED neutron interact with themselves and with hadrons will open up another avenue to explore the interplay between species from the same branch and from different branches of the quark family of the Standard Model. Furthermore, the possibility of the many-body interaction between QED dark neutrons forming a bound multi-QED-neutron system and the interaction between the QED neutron matter and other standard QCD matter will add other dimensions to the complexity of matter associated with

the QED dark neutron. It will be of great interest to extend the frontier of QED neutrons both theoretically and experimentally.

8 Acknowledgments

The author would like to thank Profs. H. Georgi, Y. Jack Ng, Lai-Him Chan, A. Koshelkin, Gang Wang, H. Sazdjian, G. Wilk, Pisin Chen, Larry Zamick, Jia-Chao Wang, Scott Willenbrock, and J. Stone for helpful communications and discussions. The research was supported in part by the Division of Nuclear Physics, U.S. Department of Energy under Contract DE-AC05-00OR22725.

Appendix A: Schwinger's boson and massless fermions in 1+1 dimensional QED

Our goal is to study the stability of color-singlet states involving three light quarks in QED interactions. To pave the way for such an investigation, we would like to sharpen our theoretical tools by examining the analogous two-body problem of a massless fermion-antifermion pair in QED, for which the exact solution from Schwinger is already known [54,55].

Schwinger showed previously that in 1+1 dimensions, massless fermions and antifermions interacting with the QED gauge interaction with a coupling constant $e=e_{2D}\equiv g_{2D}^{\text{QED}}$ give rise to a bound boson with a mass m , given by [54,55]

$$m = \frac{e}{\sqrt{\pi}}, \quad (\text{A.1})$$

where the QED coupling constant e has the dimension of a mass in 1+1 dimensions. In terms of the description of e as a unit of charge and Q as the charge number, the fermion can be described as possessing a charge e and a charge number $Q = 1$ and the antifermion a charge $(-e)$ and a charge number $Q = (-1)$ in the Schwinger model.

A derivation of Schwinger's exact solution of (A.1) can be found in [55] and explained in details in Chapter 6 of [98]. Recent generalizations and extensions of the Schwinger model have been presented in [99,100,101]. It is illuminating to review its salient points here to see in what way we may treat Schwinger's boson as a relativistic two-body problem. Schwinger's exact solution can be obtained self-consistently as a many-body field theory problem involving the response of all fermions in the presence of a perturbing gauge field A^μ . We start by considering a vacuum state in which all the negative-energy states of the massless fermions in the

Dirac sea are occupied. A disturbance in the fermion density and/or fermion current j^μ will generate a perturbing gauge field A^μ . The presence of the perturbing A^μ induces a change of the gauge phases of fermion field operator ψ through the Dirac equation

$$\gamma_\mu(i\partial_\mu - eA^\mu)\psi(x) = 0, \quad (\text{A.2})$$

where γ^μ are the gamma matrices in 1+1 dimensions. The change of the gauge phases of fermion field operator ψ in turn lead to a change of the fermion current j^μ . By imposing the Schwinger modification factor, $e^{ie \int_{x'}^x A_\mu(\xi) d\xi^\mu}$, to ensure the gauge invariance of the fermion Green's function, the induced fermion current j^μ is given implicitly as a function of the perturbing gauge field A^μ by

$$j^\mu(x) = \frac{-e}{2} \left\{ \lim_{\substack{x^0=x^0' \\ x^1=x^1'-\epsilon}} + \lim_{\substack{x^0=x^0' \\ x^1=x^1'+\epsilon}} \right\} \text{tr} \left[e^{ie \int_{x'}^x A_\mu(\xi) d\xi^\mu} \times \langle T(\bar{\psi}(x')\gamma^\mu\psi(x)) \rangle \right], \quad (\text{A.3})$$

where T is the time-order operator. Upon evaluating the above limits from the left and from the right at the space-time point $x = (x^0, x^1)$, the fermion current singularities from the left and from the right cancel and the induced gauge-invariant fermion current j^μ is found to be related explicitly to the perturbing gauge field A^μ by

$$j^\mu = -\frac{e}{\pi} \left[A^\mu - \partial^\mu \frac{1}{\partial^\lambda \partial_\lambda} \partial_\nu A^\nu \right]. \quad (\text{A.4})$$

The resultant fermion current j^μ in turn leads to a new gauge field \tilde{A}^μ , through the Maxwell equation,

$$\partial_\nu F^{\mu\nu} = \partial_\nu (\partial^\mu \tilde{A}^\nu - \partial^\nu \tilde{A}^\mu) = e j^\mu. \quad (\text{A.5})$$

From Eqs. (A.4) and (A.5), the self-consistency of the resultant gauge field \tilde{A}^μ matching the initial perturbing gauge field A^μ leads to the gauge field satisfying the Klein-Gordon equation

$$-\square A^\mu - \frac{e^2}{\pi} A^\mu = 0. \quad (\text{A.6})$$

Therefore, massless fermions and antifermions interacting non-perturbatively in a gauge field with a coupling constant e in 1+1 dimensions result in a boson field with a quanta of mass $m=e/\sqrt{\pi}$.

It is clear from the above review that the exact solution of the boson state does not lend itself readily to a simple quantum mechanical two-body problem of valence fermion (quark) and valence antifermion (antiquark) involving a simple fundamental two-body interaction, because it involves concepts of massless fermions, gauge invariance, gauge field self-consistency, and the cancellation of the fermion current singularities that are beyond the conventional two-body problems with

a simple two-body interaction. In spite of this being the case, it is desirable to construct a phenomenological two-body model for the valence fermion and antifermion with an effective interaction Φ that can be calibrated to contain the basic properties of the theory and to yield Schwinger's exact result. Examples of such an approach can be found in the successes of relativistic and non-relativistic hadron spectroscopy where the non-perturbative QCD solution involving the lattice gauge theory is approximated by a two-body theory with phenomenological effective interactions (see for example, [122, 123, 124, 125, 126, 104, 105, 106, 107, 108, 110]). Being a phenomenological two-body theory, such a theory and its generalizations will need to be worked out with considerable theoretical support and persistent confrontation with experiments so that it can be refined and readjusted, should new experimental data and new theoretical predictions become available. The present investigation on the stability of the QED neutron represents an exploration along such lines.

An additional advantage of a successful phenomenological two-body problem treatment rests on its ability to simplify the calculations, to retain the essential features, to provide an intuitive understanding, and to help solve problems that may not be solvable in a full treatment of the field theory, paving the way for our analysis on the stability of the three-quark system in section 2.

Appendix B: The separation and the independence of the color-singlet and color-octet $q\bar{q}$ excitations

It is instructive to review how the color-singlet and color-octet $q\bar{q}$ excitations can arise in a quark-QCD-QED system. We start with the quark-QCD-QED vacuum which is the lowest energy state with quarks filling up the negative-energy Dirac sea and interacting in QCD and QED interactions. We introduce a disturbance which creates one or many $q\bar{q}$ pairs, as for example, (i) during the de-excitation of a highly-excited nuclear state with a proton pulling outside an alpha particle core, (ii) in a high-energy nuclear collision, or (iii) in an excited system of a quark and an antiquark stretching out from each other at high energies after the annihilation of a high energy e^+e^- pair, as represented schematically by Figs. (1a), (1b), and (1c) of [33]. Final state interactions allow the creation of only those final $q\bar{q}$ states at eigenenergies of the QCD or QED mesons because the density of final states away from the meson eigenenergies is zero on account of the confinement of quarks.

We focus our attention on one of the lowest energy produced $q\bar{q}$ pairs. For the created $q\bar{q}$ pair to be in

a QCD or QED meson state, there must be a direction of dominant motion of the quark and the antiquark which can be taken to be the longitudinal direction. We can infer the occurrence of transverse confinement of the created $q\bar{q}$ pair and the created QCD and QED gauge fields at the moment of their creation, from Polyakov's results of the confinement of opposite charges in compact Abelian and non-Abelian gauge theories in (2+1)D [80,81]. The cylindrical flux tube arising from the subsequent longitudinal stretching of the initial quark and antiquark will remain transversely confined, as discussed in [29,33]. We can thus study the longitudinal dynamics of the quark and the antiquark system by idealizing the cylindrical flux tube as a one-dimensional string in (1+1)D, with its information on the transverse flux tube radius R_T stored in the new gauge field coupling constant $g=g_{2D}=g_{4D}/\sqrt{\pi}R_T$ in (1+1)D, and its transverse quark mass m_T obtained from the eigenvalue of a transverse equation of motion of the quark in the flux tube [28,31,34]. Because the masses of light quarks are small, it is reasonable to assume light quarks to be massless so that Schwinger's model of massless charges can be applied.

We are now in a position to examine the color degrees of freedom in the longitudinal dynamics of quarks and antiquarks in a general quark-QCD-QED system in the idealized (1+1)D. As we mentioned in the Introduction, the quark current j^μ and the gauge fields A^μ are not single-element functions. They are in fact 3×3 color matrices. Quarks in color-triplet $\mathbf{3}$ representation and antiquarks in color $\mathbf{3}^*$ representation form the product group of $\mathbf{3} \otimes \mathbf{3}^* = \mathbf{1} \oplus \mathbf{8}$, which contains the color-singlet $\mathbf{1}$ subgroup and the color-octet $\mathbf{8}$ subgroup of generators.

In the general case, the color-octet QCD gauge fields $A^\mu(x) = \sum_{i=1}^8 A_i^\mu(x)t^i$ contains eight non-Abelian degrees of freedom and their couplings will lead to color excitations, the majority of which will not lead to stable collective excitations. To get stable collective excitations, we represent the color-octet degrees of freedom by a single unit vector τ^1 oriented randomly in the eight-dimensional $SU(3)$ color generator space [28,31,34],

$$\tau^1 = \sum_{i=1}^8 n_a t^a, \quad \text{with} \quad \sqrt{n_1^2 + n_2^2 + \dots + n_8^2} = 1, \quad (\text{B.7})$$

where $n_a = 2\text{Tr}\{\tau^1 t^a\}$, and we restrict the dynamics of the QCD gauge fields only to the gauge field amplitude $A_1^\mu(x)$ along the τ^1 direction, while keeping the τ^1 orientation fixed. The gauge fields of the quark-QCD-QED system are then described by the color-singlet amplitudes $A_0^\mu(x)$ for QED dynamics and the color-octet

amplitude $A_1^\mu(x)$ for QCD dynamics as [28,31,34]

$$A^\mu(x) = A_0^\mu(x)\tau^0 + A_1^\mu(x)\tau^1 = \sum_{\lambda=0}^1 A_\lambda^\mu(x)\tau^\lambda, \quad (\text{B.8})$$

where $\tau^0 = t^0$, $2\text{Tr}(\tau^\lambda \tau^{\lambda'}) = \delta^{\lambda\lambda'}$, and $\lambda, \lambda' = 0, 1$. The quark currents $j^\mu(x)$ can be likewise represented by the color-singlet and color-octet current components as

$$j^\mu(x) = j_0^\mu(x)\tau^0 + j_1^\mu(x)\tau^1 = \sum_{\lambda=0}^1 j_\lambda^\mu(x)\tau^\lambda. \quad (\text{B.9})$$

Because τ^0 and τ^1 commute, the gauge fields in this restricted subspace are Abelian.

We can now examine the dynamics of the quarks fields and the gauge fields. We start with initial gauge fields A_λ^μ which affect the quark field. The Dirac equation (A.2) for the quark field is

$$\gamma_\mu \left(i\partial^\mu + \sum_{\lambda=0}^1 g^\lambda A_\lambda^\mu(x)\tau^\lambda \right) \psi(x) = 0. \quad (\text{B.10})$$

After obtaining the solutions to the above Dirac equation for the quark field $\psi(x)$, we evaluate the quark current $j_\lambda^\mu(x)$ as a function of the applied initial gauge field $A_\lambda^\mu(x)$,

$$j_\lambda^\mu(x) = \frac{1}{2} \left\{ \lim_{\substack{x^0=x^0' \\ x^1=x^1'-\epsilon}} + \lim_{\substack{x^0=x^0' \\ x^1=x^1'+\epsilon}} \right\} \text{tr} \left[e^{i \int_{x^1}^{x^1'} \sum_{\lambda'}^1 (-g^{\lambda'}) A_{\lambda'}^\mu(\xi) \tau^{\lambda'} d\xi_\mu} \langle T(\bar{\psi}(x') \gamma^\mu \tau^\lambda \psi(x)) \rangle \right]. \quad (\text{B.11})$$

The induced quark current $j_\lambda^\mu(x)$ as a function of the initial applied gauge field A_λ^μ is found to be [34]

$$j_\lambda^\mu(x) = \frac{g^\lambda}{\pi} \left(A_\lambda^\mu(x) - \frac{\partial_\nu \partial^\mu}{\partial^2} A_\lambda^\nu(x) \right), \quad (\text{B.12})$$

where $\lambda=0$ for QED, $\lambda=1$ for QCD. We note specially that in the above Eq. (B.12), the induced current $j_\lambda^\mu(x)$ of type λ depends only on the initial gauge field $A_\lambda^\mu(x)$ of same type λ and does not depend on the gauge field of the other type, even though both types of gauge fields are present in the sum over λ' in the Schwinger gauge-invariant exponential factor. Such a dependence (and independence) arises because in obtaining the above result in Eq. (B.12), we expand the Schwinger gauge-invariant exponential factor in Eq. (B.11), and take the trace over the color space involving the $\tau^{\lambda'}$ generator from the Schwinger factor, and the τ^λ generator from $T\langle \bar{\psi} \gamma^\mu \tau^\lambda \psi \rangle$. Because of the orthogonality of the color generators, $2\text{tr}\{\tau^{\lambda'} \tau^\lambda\} = \delta^{\lambda'\lambda}$, the contribution from the interaction of the other type is zero [34]. In physical terms, the above mathematical result means that to be observable a color-singlet quark density oscillation must

remain colorless⁴ and cannot become colored, when the color-singlet quark density oscillation absorbs a gauge boson. Hence, it can only absorb a QED gauge boson A_0^μ but not a QCD gauge boson A_1^μ to make the color-singlet quark density oscillation observable. On the other hand, a color-octet quark density $j_1^\mu(x)$ oscillation cannot become observable until it bleaches its octet color to become colorless. Hence it can only absorb a QCD gauge boson A_1^μ but not a QED gauge boson A_0^μ to make the color-octet quark density $j_1^\mu(x)$ oscillation observable. Therefore, in the collective dynamics of the quark-QCD-QED medium, quark currents of the type λ , $j_\lambda^\mu(x)$, is affected only by gauge fields of the same type λ , $A_\lambda^\mu(x)$, as shown in Eq. (B.12).

The induced quark current $j_\lambda^\mu(x)$ generates a new gauge fields $\tilde{A}_\lambda^\mu(x)$ through the Maxwell equation, which in the Abelian approximation of Eq. (B.8) is

$$-\partial_\nu \partial^\nu \tilde{A}_\lambda^\mu(x) + \partial_\nu \partial^\mu \tilde{A}_\lambda^\nu(x) = g^\lambda j_\lambda^\mu(x). \quad (\text{B.13})$$

Stable self-consistent collective dynamics of the quark field and the gauge fields can be obtained when the newly generated gauge fields \tilde{A}_λ^μ are the same as the initial applied gauge fields A_λ^μ . Such self-consistency can be achieved by setting $\tilde{A}_\lambda^\mu = A_\lambda^\mu$ and substituting Eq. (B.13) into Eq. (B.12). We get the Klein-Gordon equation for the currents

$$-\partial^\nu \partial_\nu j_\lambda^\mu = m_\lambda^2 j_\lambda^\mu, \quad (\text{B.14})$$

which corresponds to the occurrence of a boson of a stable and independent collective excitation of the quark-QCD-QED medium, with a mass m_λ given by

$$m_\lambda^2 = \frac{(g^\lambda)^2}{\pi}, \quad \begin{cases} \lambda = 0 & \text{for QED} \\ \lambda = 1 & \text{for QCD} \end{cases}. \quad (\text{B.15})$$

From another perspective, the separation and the independence of the color-singlet and the color-octet excitations are possible because the gauge-invariant relations between the charge currents j^μ and the gauge fields A^μ in (1+1)D in Eqs. (A.4) and (A.5) (and similarly in Eqs. (B.12) and (B.13)) are each a linear function of j^μ and A^μ . As a consequence, there is a principle of superposition of currents and gauge fields of different color components in color-space. Thus, the quark-QCD-QED medium possesses stable and independent collective QCD and QED excitations with different bound states masses m_λ , depending on the coupling constants g^λ . From Eq. (B.15), the ratio of the QED meson mass

⁴The physical quark density is the time-component of the quark current, $j_\lambda^0(x)$, and its temporal dependence gives the quark density oscillation. In mathematical terms, the observability of the quark density oscillation corresponds to a non-zero value of the quark current upon taking the trace over the color space.

to the QCD meson mass is of order

$$\frac{m_{\text{QED meson}}}{m_{\text{QCD meson}}} \sim \frac{g^{\text{QED}}}{g^{\text{QCD}}} \sim \sqrt{\frac{\alpha_{\text{QED}}}{\alpha_{\text{QCD}}}} \sim \sqrt{\frac{1/137}{0.6}} \sim \frac{1}{9}, \quad (\text{B.16})$$

which is Eq. (1).

Appendix C: Relativistic two-body problem

The relativistic two-body wave equations for the wave function Ψ for QED interactions in 1+1 dimensions consist of two mass-shell constraints on each of the interacting particles [104, 105, 106, 107, 108, 109, 110, 111, 112],

$$\mathcal{H}_1|\Psi\rangle = \left\{ p_1^2 - m_1^2 - \Phi_{12}(x_{12}) \right\} |\Psi\rangle = 0, \quad (\text{C.17a})$$

$$\mathcal{H}_2|\Psi\rangle = \left\{ p_2^2 - m_2^2 - \Phi_{21}(x_{21}) \right\} |\Psi\rangle = 0. \quad (\text{C.17b})$$

As emphasized in Appendix A, Schwinger's exact solution in field theory resulting in longitudinal confinement is in fact the solution of the collective motion for a many-body problem of great complexity. It is not a simple two-body problem of a fundamental interaction. In transcribing the Schwinger field theory problem as a phenomenological two-body problem, there are choices of different forms of the two-body effective interaction. An alternative form uses the QED confining linear interaction in the Coulomb gauge as the time-like vector potential $V_{12}(r)$ in a minimum substitution form, and it leads to $[(p_i^0 - V_{12}(x_{12}))^2 - \mathbf{p}_i^2 - m_0^2] \Psi = 0$. However, such an effective interaction has the unpleasant feature that the V_{12}^2 term in the above Schrödinger-type equation leads to solutions whose behavior do not match the behavior of the Schwinger solution at large separations. It becomes necessary to introduce an additional scalar confining interaction $S_{12}(x_{12})$ so that the wave equation becomes $[(p_i^0 - V_{12}(x_{12}))^2 - \mathbf{p}_i^2 - (m_0^2 + S_{12}(x_{12}))^2] \Psi = 0$. The choice of $V_{12} = S_{12}$ used in [109] leads to a cancellation of the V_{12}^2 term with the S_{12}^2 term at large separations and a total effective interaction similar to the Φ used here. In view of the phenomenological nature of the confining interaction, the present effective confining interaction Φ_{12} in Eq. (C.17b) serves well as a description that can match the confinement property of the Schwinger solution.

We would like to calibrate the above effective interaction Φ_{ij} by comparing the solution of the above two-body problem with Schwinger's exact QED solution in 1+1 dimensions. We construct the total Hamiltonian \mathcal{H} from these constraints by

$$\mathcal{H} = \sum_{i=1}^2 \mathcal{H}_i. \quad (\text{C.18})$$

In order that each of these constraints be conserved in time we must have

$$[\mathcal{H}_i, \mathcal{H}]|\psi\rangle = i \frac{d\mathcal{H}_i}{d\tau} |\Psi\rangle = 0. \quad (\text{C.19})$$

As a consequence, the above equation leads to the compatibility condition between the two constraints [104, 105, 106, 107, 108, 109, 110],

$$[\mathcal{H}_i, \mathcal{H}_j]|\Psi\rangle = 0. \quad (\text{C.20})$$

Since the masses m_1 and m_2 commute with the operators, this implies

$$\left([p_1^2 \Phi_{21}(x_{21})] - [p_2^2 \Phi_{12}(x_{12})] \right) |\Psi\rangle = 0. \quad (\text{C.21})$$

The above equation cannot be satisfied if $\Phi_{12}(x_{12}) \neq \Phi_{21}(x_{21})$. The simplest way to satisfy the above equation is to take

$$\Phi_{12}(x_{12}) = \Phi_{21}(x_{21}) = \Phi(x_{12}), \quad (\text{C.22})$$

which is the relativistic analogue of Newton's third law. The compatibility condition (C.21) then requires the effective interaction $\Phi(x_{12})$ to depend only on the coordinate $x_{12\perp}$ transverse to the total momentum $P=p_1+p_2$, $\Phi(x_{12}) = \Phi(x_{12\perp})$,

$$(\text{C.23})$$

where $x_{12\perp} = (x_1 - x_2) - \frac{(x_1 - x_2) \cdot P}{P^2} P$.

$$(\text{C.24})$$

We shall work in the CM system where the total momentum P is $(P^0, P^1) = (M, 0)$, M is the invariant mass of the composite system, and the relative coordinate $x_{ij\perp} = (x_1 - x_2)$ involves only spatial coordinates x_1 and x_2 . The particle momentum p_i can be separated out into a component ϵ_i parallel to P and a component q_i transverse to P as

$$p_i = (\epsilon_i, q_i) = \epsilon_i \frac{P}{\sqrt{P^2}} + q_i, \quad i = 1, 2, \quad (\text{C.25})$$

where $\epsilon_i = \frac{p_i \cdot P}{\sqrt{P^2}}$, and $q_1 + q_2 = 0$.

$$(\text{C.26})$$

In terms of ϵ_i , the invariant mass of the composite system M is given by

$$M = P^0 = \epsilon_1 + \epsilon_2. \quad (\text{C.27})$$

The two-body wave equations (C.17a) and (C.17b) in the CM system becomes

$$\epsilon_1^2 |\Psi\rangle = \{q_1^2 + m_1^2 + \Phi(x_{12\perp})\} |\Psi\rangle, \quad (\text{C.28a})$$

$$\epsilon_2^2 |\Psi\rangle = \{q_2^2 + m_2^2 + \Phi(x_{12\perp})\} |\Psi\rangle. \quad (\text{C.28b})$$

Because $q_2 = (-q_1)$, the second equation of the above is simply

$$(\epsilon_2^2 - \epsilon_1^2) |\Psi\rangle = (m_1^2 - m_2^2) |\Psi\rangle. \quad (\text{C.29})$$

It is only necessary to solve for the eigenstate of the first Schrödinger-type equation (C.28a) to obtain ϵ_1 , and the quantity ϵ_2 can be obtained as an algebraic equation from (C.29). The knowledge of ϵ_1 and ϵ_2 (taken to be positive) then gives the invariant mass M of the interacting two-body system.

Appendix D: Schwinger's QED boson as a relativistic two-body problem in 1+1 dimensions

The brief summary presented in Appendix A makes it plain that the Schwinger boson that is confined and bound in 1+1 dimensions is in fact a non-linear self-consistent solution of a many-body system of great complexity. It is desirable to construct a phenomenological two-body problem for QED in 1+1 dimensions involving a valence fermion and a valence antifermion with an effective phenomenological interaction $\Phi(x_{12\perp})$ that can be calibrated to contain the basic properties of the theory and to yield Schwinger's exact QED result in 1+1 dimensions.

Accordingly, we consider the two-body wave equations (C.28a) and (C.28b) (or (C.29)) in the CM system for two charge particles with charge numbers Q_1 and Q_2 , interacting with a phenomenological effective QED interaction $\Phi(x_{12\perp})$

$$\Phi(x_{12\perp}) = \frac{2\epsilon_1\epsilon_2}{\epsilon_1 + \epsilon_2} (-Q_1 Q_2) \kappa |x_1 - x_2|. \quad (\text{D.30})$$

The effective QED interaction $\Phi(x_{12\perp})$ in 1+1 dimensions has been chosen such that:

1. In the Coulomb gauge, the interaction energy between charges $Q_1 e$ and $Q_2 e$ in 1+1 dimensional QED is $(-Q_1 Q_2 e^2 / 2) |x_1 - x_2|$ [57], which is indeed confining for the attractive interaction between unlike charges. It is reasonable to use such a spatially linear interaction in the phenomenological two-body problem. The value of the coefficient parameter κ of such a linear potential in (D.30) will be affected by the use of the phenomenological reduced mass factor, Schwinger's self-consistency condition on the gauge field, and the gauge invariance constraint. It is therefore appropriate to extract κ phenomenological from Schwinger's exact solution.
2. The quantity κ is proportional to the square of the coupling constant e^2 . The exact value of κ will be chosen to give Schwinger's solution of $m = e/\sqrt{\pi}$ for a massless fermion-antifermion pair interacting in the QED interaction.
3. The effective interaction contains the charge factor $(-Q_1 Q_2)$, which leads to an attractive interaction if $Q_1 Q_2 < 0$, and a repulsive interaction if $Q_1 Q_2 > 0$, as in standard QED interaction in quantum electrodynamics.
4. The reduced mass factor $2(\epsilon_1 \epsilon_2) / (\epsilon_1 + \epsilon_2)$ has been chosen to give the proper reduced mass in the non-relativistic two-body wave equation. We have however used the particle energy ϵ_i in lieu of the rest mass m_i , to make it applicable also to the massless limit. The reduced mass factor depends on the

eigenvalues ϵ_i which should be self-consistently determined by the wave equations (C.28a) and (C.28b).

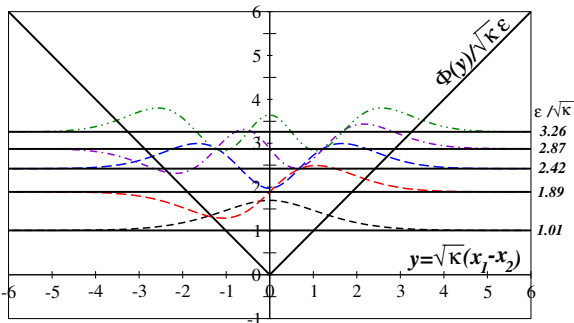


Fig. 7 The solid curve gives the phenomenological effective potential $\Phi(y)/\sqrt{\kappa}\epsilon$ for a fermion and an antifermion interacting in the QED two-body problem in 1+1 dimensions. The energies of the lowest five eigenstates are indicated by horizontal lines with their corresponding wave functions $\Psi(y)$ as curves on these lines. The parameter κ in the phenomenological effective potential $\Phi(y)/\sqrt{\kappa}\epsilon$ is obtained by matching the solution for the lowest-energy state of the two-body problem with Schwinger's exact solution.

Our present task is to obtain the eigenstates for the wave equation (C.28a) with the effective potential of (D.30). Schwinger's case of massless fermion and antifermion corresponds to $Q_1=1$, $Q_2=-1$, $m_1=m_2=0$, $\epsilon_1=\epsilon_2=\epsilon$, and $M=2\epsilon$. Using the dimensionless variable

$$y = \sqrt{\kappa}(x_1 - x_2), \quad (\text{D.31})$$

the effective interaction $\Phi(y)/\kappa$ is then

$$\frac{\Phi(y)}{\kappa} = \frac{\epsilon}{\sqrt{\kappa}}|y|, \quad (\text{D.32})$$

and the wave equation (C.28a) becomes

$$\left\{ -\frac{\partial^2}{\partial y^2} + \frac{\epsilon}{\sqrt{\kappa}}|y| - \frac{\epsilon^2}{\kappa} \right\} \Psi(y) = 0. \quad (\text{D.33})$$

We show in Fig. 7 the dimensionless effective potential, $\Phi(y)/\sqrt{\kappa}\epsilon$, expressed in units of $\sqrt{\kappa}\epsilon$. It is a linearly-rising function of the dimensionless spatial separation $|y|$ between the charges, expressed units of $1/\sqrt{\kappa}$. The solution of the wave equation with a linearly rising interaction is the Airy function. The wave equation (D.33) becomes the Airy equation

$$\left\{ \frac{\partial^2}{\partial z^2} - \left(|z| - \left(\frac{\epsilon}{\sqrt{\kappa}} \right)^{4/3} \right) \right\} \Psi(z) = 0, \quad (\text{D.34})$$

$$\text{where } z = \left(\frac{\epsilon}{\sqrt{\kappa}} \right)^{1/3} |y|. \quad (\text{D.35})$$

The solution satisfying the boundary condition at large $|y|$ is

$$\Psi(z) = \text{Ai}\left(|z| - \left(\frac{\epsilon}{\sqrt{\kappa}} \right)^{4/3}\right). \quad (\text{D.36})$$

The eigenstate is obtained by matching the wave function and its derivative at $z=0$. There are two types of eigenstates with even and odd parities:

$$\text{even parity: } \Psi'(z)|_{z=0} = \text{Ai}'\left(-\left(\frac{\epsilon}{\sqrt{\kappa}}\right)^{4/3}\right) = 0, \quad (\text{D.37})$$

$$\text{odd parity: } \Psi(z)|_{z=0} = \text{Ai}\left(-\left(\frac{\epsilon}{\sqrt{\kappa}}\right)^{4/3}\right) = 0. \quad (\text{D.38})$$

We label the locations where the wave function or its derivative are zero as $(-a_s)$ with $\text{Ai}(-a_s) = 0$ or $\text{Ai}'(-a_s) = 0$. Then the eigenvalues of the wave equations ϵ are given by

$$\left(\frac{\epsilon}{\sqrt{\kappa}} \right)^{4/3} = a_s, \quad \text{or} \quad \epsilon = a_s^{3/4} \sqrt{\kappa}. \quad (\text{D.39})$$

Table 2 Solution of the two-body problem with the effective interaction $\Phi(y)/\sqrt{\kappa}\epsilon$ for the lowest states. Here n is the number of nodes of the two-body wave function, and $M/\sqrt{\kappa}$ is the dimensionless measure of the composite particle mass.

n	Parity	a_s	$\epsilon/\sqrt{\kappa}$	$M/\sqrt{\kappa}$	$\sqrt{\langle y^2 \rangle}$	$\sqrt{\langle q_1^2 \rangle}/\sqrt{\kappa}$
0	even	1.02	1.01	2.02	0.862	0.60
1	odd	2.34	1.89	3.98	1.38	1.09
2	even	3.25	2.42	4.84	1.78	1.41
3	odd	4.09	2.87	5.74	2.10	1.66
4	even	4.82	3.26	6.50	2.38	1.89

Table 2 gives the values of a_s , (energy ϵ)/ $\sqrt{\kappa}$, (mass M)/ $\sqrt{\kappa}$, $\sqrt{\langle y^2 \rangle}$, and $\sqrt{\langle q_1^2 \rangle}/\sqrt{\kappa}$ of the lowest five states. Fig. 7 displays the energies as the horizontal lines, with their corresponding wave functions $\Psi(y)$ exhibiting different number of nodes. In the two-body problem with the phenomenological two-body interaction, the mass of the lowest state for the phenomenological potential is $M = 2.02\sqrt{\kappa}$. On the other hand, the Schwinger's exact solution (A.1) in field theory gives $M = e/\sqrt{\pi}$. Therefore, by matching the mass of the lowest eigenstate from the phenomenological two-body theory with the mass from Schwinger's field theory, we find κ to be

$$\kappa = \frac{e^2}{4.08\pi} \sim \frac{e^2}{4\pi}, \quad (\text{D.40})$$

where for simplicity, we shall approximate the denominator 4.08π to be 4π . We have thus obtained the phenomenological interaction Φ in Eq. (D.30) between two electric charges interacting in QED in 1+1 dimensions. Such a knowledge of the effective QED interaction between two electric charges will enable us to study the states of three quarks interacting in 1+1 dimensional QED.

We need the value of the coupling constant $e = e_{2D}$ which can be obtained from e_{4D} . In the physical world of

3+1 dimensions, the one-dimensional open string without a structure is in fact an idealization of a flux tube with a transverse radius R_T . The masses calculated in 1+1 dimensions can represent physical masses, when the structure of the flux tube is properly taken into account. Upon considering the structure of the flux tube in the physical 3+1 dimensions, we find that the coupling constant e_{2D} in 1+1 dimensions is related to the physical coupling constants e_{4D} in 3+1 dimensions by the flux tube radius R_T , [28, 31, 84, 69, 34]

$$(e_{2D})^2 = \frac{1}{\pi R_T^2} (e_{4D})^2 = \frac{4\alpha_{4D}}{R_T^2}, \quad (\text{D.41})$$

with $\alpha_{4D} = 1/137$ and $R_T = 0.4$ fm [31], which yields $\sqrt{\kappa} = 23.8$ MeV, and $\hbar/\sqrt{\kappa} = 8.3$ fm.

As a final check of a faithful representation of the phenomenological two-body model for the Schwinger exact field theory in 1+1 dimensions, we note that they share the distinct property that the mass of the system increases with the increase in the magnitude of the coupling constant, in contrast to a non-confining interaction such as the positronium where the mass of the composite system decreases with the increase in the magnitude of the coupling constant.

We note from the above solutions of the two-body problem that a fermion-antifermion composite system with the phenomenological QED interaction possesses excited states with a higher number of nodes n , in addition to the lowest state with $n = 0$. They represent higher string vibrational excitations of the fermion-antifermion system as an open string. As a rough guide for future searches of QED meson states in $(q\bar{q})$ composite systems, we can treat the observed X17 state at $E = 16.70$ MeV [10] to be the lowest band heads of the $(I = 0, n = 0)$ state, and the E38 state at $E = 37.38$ MeV [14] to be the lowest band heads of the $(I = 1, I_3 = 0, n = 0)$ state respectively. We can then use the QED meson solutions as displayed in Fig. 7 and Table 2 to build on these two band heads semi-empirically an approximate theoretical energy level diagram for QED meson states with higher numbers of nodes n , as shown in Fig. 8. On the right panel of Fig. 8, we also display the decay energy $E(I = 0, n + 1) - E(I = 0, n)$ for the transition from the $(I = 0, n + 1)$ state to the $(I = 0, n)$ state. This decay energy corresponds to the diphoton energy if the $(I = 0, n + 1)$ state decays into the (I, n) state with the emission of two real or virtual photons as indicated in the diagram Fig. 10(b) and 10(c) below. Future experimental searches for these two-body excited states and their diphoton decays in QED mesons will be of great interest. It should be emphasized that the spectrum shown in Fig. 8 is useful as an initial guide as many effects such as the fine structure of the states

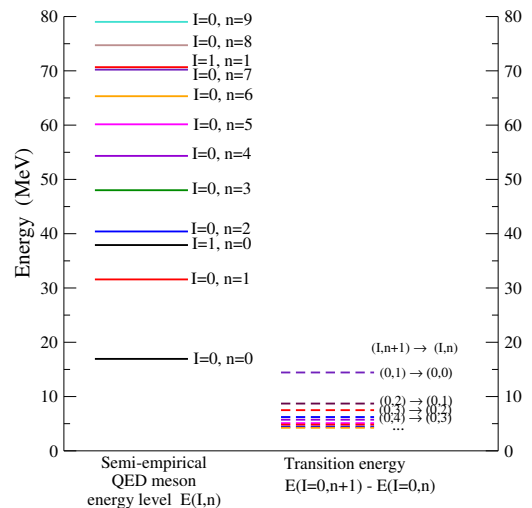


Fig. 8 The left panel gives the semi-empirical QED meson energy level $E(I, n)$ where I is the isospin quantum number and n is the number of nodes, as obtained from Fig. 7 and Table I by assuming the observed X17 state at 16.70 MeV [10], as the band heads of the $(I = 1, n = 0)$ and the E38 state at $E = 37.38$ MeV [14] as the band head of the $(I = 1, I_3 = 0, n = 0)$ states respectively. The right panel gives the transition energy $E(I = 0, n + 1) - E(I = 0, n)$ as dashed lines.

and the deviations from the linear potential shape may modify the spectrum.

Appendix E: Variational Calculation for the lowest two-body bound state energy

Before we apply the effective interaction $\Phi_{12}(x_{12})$ to the three-quark problem, we wish to test here whether a variational calculation using the effective interaction (D.30) will also lead to the same two-body bound state mass for the lowest-energy two-body state. The success of the variational calculations will pave the way in a similar variational calculation for the three-body problem in section 2. We therefore evaluate the lowest two-body bound state energy by using a Gaussian variational wave function. For massless quarks with $Q_1 = 1$, $Q_2 = -1$, we rewrite (D.33) as

$$\{\mathcal{H}_0 - E^2\} |\psi\rangle = 0, \quad (\text{E.42})$$

$$\text{where } \mathcal{H}_0 = -\frac{\partial^2}{\partial y^2} + E|y|, \quad \text{and } E = \frac{\epsilon}{\sqrt{\kappa}}. \quad (\text{E.43})$$

We introduce a Gaussian variational wave function with the variational parameter σ ,

$$\Psi(y) = \left(\frac{1}{\sqrt{2\pi}\sigma}\right)^{1/2} \exp\left\{-\frac{y^2}{4\sigma^2}\right\} = N \exp\left\{-\frac{y^2}{4\sigma^2}\right\}. \quad (\text{E.44})$$

We obtain

$$\langle \mathcal{H}_0 \rangle(\sigma) = \frac{1}{4\sigma^2} + \frac{2\sigma E}{\sqrt{2\pi}}. \quad (\text{E.45})$$

From the requirement of $\delta\langle\mathcal{H}_0\rangle(\sigma)/\delta\sigma = 0$, we get

$$\sigma = \left(\frac{\sqrt{2\pi}}{4E}\right)^{1/3}, \quad (\text{E.46})$$

at which

$$\langle\mathcal{H}_0\rangle = \frac{3E}{\sqrt{2\pi}}. \quad (\text{E.47})$$

From Eq. (E.43), the value of E^2 at the equilibrium value of σ becomes

$$E^2 = \langle\mathcal{H}_0\rangle = \frac{3\sigma E}{\sqrt{2\pi}}. \quad (\text{E.48})$$

Eliminating σ from Eqs. (E.46) and (E.48) we get

$$E = \left(\frac{3}{(\sqrt{2\pi})^{2/3}4^{1/3}}\right)^{3/4} = 1.034 \quad (\text{E.49})$$

$$\sigma = \left(\frac{\sqrt{2\pi}}{4E}\right)^{1/3} = 0.876. \quad (\text{E.50})$$

The above variational calculation gives $E = \epsilon/\sqrt{\kappa} \sim 1$ as given in (E.49), and thus

$$\epsilon = \sqrt{\kappa}, \quad \text{and} \quad M = 2\epsilon = \frac{e}{\sqrt{\pi}}, \quad (\text{E.51})$$

which agrees with the lowest eigenenergy obtained by solving the wave equation directly. We find indeed that the variational calculation can give the correct lowest-energy bound state mass. This justifies the use of the variational calculations in the three-body problem to obtain the lowest-energy state of a QED neutron in section 2.

Appendix F: The decay and detection of composite $q\bar{q}$ QED mesons

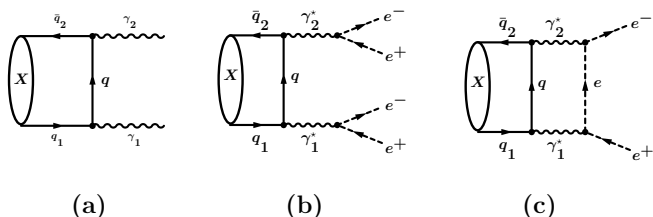


Fig. 9 Fig. 9(a) depicts the diagram for the decay of the QED meson X into two real photons ($\gamma_1\gamma_2$), Fig. 9(b) the decay of the QED meson X into two virtual photons ($\gamma_1^*\gamma_2^*$), and Fig. 9(c) the decay of the QED meson X into a dilepton (e^+e^-) pair.

We would like to review and extend here our knowledge on the decay of the QED meson [28, 31] to facilitate the experimental detection of QED mesons and the QED

neutron. We consider a $q\bar{q}$ composite system X formed by a valence quark q_1 and a valence antiquark \bar{q}_2 interacting with the effective QED interaction Φ . As shown in Appendix D, there can be many eigenstate solutions of the relativistic two-body equations for the composite system X . The additional intrinsic degrees of freedom of the quarks will add further to the complexity of the spectrum and the number of the composite particles X . In the 1+1 dimensional description, the composite particle X cannot decay, as the quarks execute a yo-yo motion along the string in an idealization of the flux tube, and the photon is represented by an effective interaction binding the quarks. In the physical 3+1 dimensions where the structure of the flux tube is taken into account and the photon decay channel opens up, the quark and the antiquark at different transverse coordinates in the tube traveling from opposing longitudinal directions can make a sharp change of their trajectories turning to the transverse direction to annihilate, leading to the emission of photons as depicted in Fig. 9(a), 9(b), and 9(c). The number of emitted photons depends on the spin and parity of the decaying system [127, 128]. We have illustrated the case of two photon decay in Fig. 9(a), 9(b), and 9(c). The emitted photon can be two real photons ($\gamma_1\gamma_2$) in 9(a), two virtual photons ($\gamma_1^*\gamma_2^*$), in 9(b), or a dilepton (e^+e^-) pair in 9(c).

There can be excited QED meson states X^* with nodal number n which can de-excite to the lower QED meson state X' with a smaller nodal number $n' < n$, with the emission of γ , $\gamma\gamma$, and $\gamma^*\gamma^*$ as shown in Fig. 10.

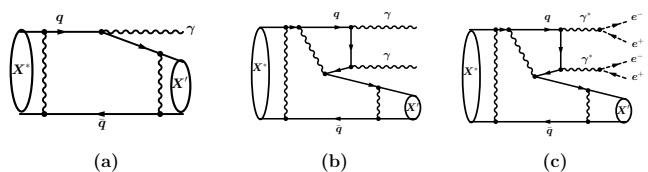


Fig. 10 Diagrams for the de-excitation of the excited QED meson X^* to the QED meson X' with particle emissions: Fig. 10(a) $X^* \rightarrow X' + \gamma$, Fig. 10(b) $X^* \rightarrow X' + \gamma + \gamma$, and Fig. 10(c) $X^* \rightarrow X' + \gamma^* + \gamma^*$.

For the decay from a bound state X , the decay amplitude needs to be folded in with the bound state momentum wave function. For $X \rightarrow k_1 + k_2$ where the final states (k_1, k_2) are (γ_1, γ_2) , (γ_1^*, γ_2^*) , or (e^+, e^-) as in diagrams 9(b), 9(c), and 9(d), the decay amplitudes are [106, 107]

$$M(X \rightarrow k_1 + k_2) = \int d^3q_1 \tilde{\Psi}(q_1) \Gamma(q_1 + \bar{q}_2 \rightarrow k_1 + k_2), \quad (\text{F.52})$$

where $\tilde{\Psi}(q_1)$ is the bound state momentum wave function of a constituent, $q_1 = q_{p_{q_1} p_{\bar{q}_2}}/2$, and $\Gamma(q_1 + \bar{q}_2 \rightarrow k_1 + k_2)$ is the Feynman amplitude for the diagram of $q_1 + \bar{q}_2 \rightarrow k_1 + k_2$, (see e.g. Eqs. (3.6) of [106] or Eq. (2.2) of [107] for the case of two-photon decay). The two-body spatial wave function $\Psi(y)$ for the QED meson X in Eqs. (D.33) has been expressed in terms of the dimensionless relative spatial coordinate $y = \sqrt{\kappa}(x_{q_1} - x_{\bar{q}_2})$. The corresponding wave function in the momentum space, $\tilde{\Psi}(q/2\sqrt{\kappa})$ is the Fourier transform of $\Psi(y)$ of Eqs. (D.32) and (D.36),

$$\tilde{\Psi}(q/2\sqrt{\kappa}) = \tilde{\Psi}(q_1/\sqrt{\kappa}) = \frac{1}{\sqrt{2\pi}} \int e^{-i(q_1/\sqrt{\kappa})y} \Psi(y) dy \quad (\text{F.53})$$

where $q = q_1 - q_2 = 2q_1$, and the constituent momentum q_1 is expressed in units of $\sqrt{\kappa}$. The momentum distribution of the composite $q_1 \bar{q}_2$ system X with a mass M is

$$\frac{dN(P, q)}{dP dq} = \delta(P^2 - M^2) |\tilde{\Psi}(q/2\sqrt{\kappa})|^2. \quad (\text{F.54})$$

We show in Figs. 11(a) the momentum wave functions $\tilde{\Psi}(q/2\sqrt{\kappa})$, and in Fig. 11(b) the corresponding momentum probability function $|\tilde{\Psi}(q/2\sqrt{\kappa})|^2$, for the lowest five states of the composite system. We can understand the contents of Eq. (F.54) intuitively as follows: the invariant square of the momentum sum, P^2 , probes the invariant mass M^2 of the composite QED meson, whereas the invariant square of the momentum difference, q^2 , measures the inverse spatial size of the decaying QED meson as $\hbar/\sqrt{\langle q^2 \rangle}$, and the number of nodes of $|\tilde{\Psi}(q/2\sqrt{\kappa})|^2$ in Eq. (F.54) and Fig. 11(b) reveals the internal structure of the composite $q_1 \bar{q}_2$ system.

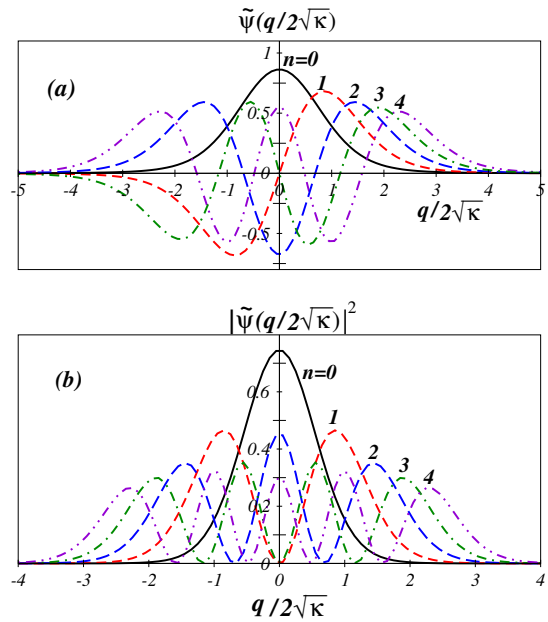


Fig. 11 Fig. 4(a) gives the two-body wave function in momentum space $\tilde{\Psi}(q/2\sqrt{\kappa})$ of the composite $q\bar{q}$ system as a function of the relative momentum $q = q_1 - q_2 = 2q_1$ in units of $2\sqrt{\kappa}$, and Fig. 4(b) gives $|\tilde{\Psi}(q/2\sqrt{\kappa})|^2$.

The decay via two virtual photons in diagram Fig. 9(b) may provide an interesting probe to yield additional information on the decaying QED meson parent particle. One can construct the invariant momenta square of the sum and differences of the 4-momenta of the two virtual photons,

$$\begin{aligned} P_{\gamma_1^* \gamma_1^*}^2 &= (p_{\gamma_1^*} + p_{\gamma_2^*})^2, \\ Q_{\gamma_1^* \gamma_1^*}^2 &= -(p_{\gamma_1^*} - p_{\gamma_2^*})^2, \end{aligned} \quad (\text{F.55})$$

and $P \equiv P_{\gamma_1^* \gamma_1^*} = \sqrt{P_{\gamma_1^* \gamma_2^*}^2}$, $Q \equiv Q_{\gamma_1^* \gamma_1^*} = \sqrt{-q_{\gamma_1^* \gamma_2^*}^2}$. Experimental measurement of the virtual diphoton pair distribution

$$\frac{dN(P_{\gamma_1^* \gamma_2^*}, q_{\gamma_1^* \gamma_2^*}^2)}{dP_{\gamma_1^* \gamma_2^*} dq_{\gamma_1^* \gamma_2^*}^2} = \frac{dN(P, Q)}{dP dQ} \quad (\text{F.56})$$

will provides useful information on the composite $q\bar{q}$ particles of massless light quarks from virtual diphoton decay measurements. Specifically, one makes a scatter plot of diphoton events on the two dimensional plane of P and Q . In actual experiments with the presence of cuts and windows in various kinematical regions, one may resort to the use of the event mixing method to normalize the distribution as

$$\left. \frac{dN(P, Q)}{dP dQ} \right|_{\text{norm}} \equiv \frac{\left[\frac{dN(P, Q)}{dP dQ} \right]_{\text{correlated}}}{\left[\frac{dN(P, Q)}{dP dQ} \right]_{\text{mixed events}}}. \quad (\text{F.57})$$

The above normalized distribution $dN(P, Q)/dP dQ|_{\text{norm}}$ is expected to cluster sharply around the invariant mass

$M = (P + Q)/2$ of the composite particles and spread out in width in the direction of Q . One can alternatively display the distribution in terms of the rotated coordinates $(P + Q)/2$ and a small stripe of $P - Q > 0$.

References

1. P.V. Chliapnikov *et al.*, Observation of direct soft photon production in π^-p interactions at 280 GeV/c, Phys. Lett. B 141, 276 (1984).
2. F. Botterweck *et al.* (EHS-NA22 Collaboration), Direct soft photon production in K^+p and π^+p interactions at 250 GeV/c, Z. Phys. C 51, 541 (1991).
3. S. Banerjee *et al.* (SOPHIE/WA83 Collaboration), Observation of direct soft photon production in π^-p interactions at 280 GeV/c, Phys. Lett. B 305, 182 (1993).
4. A. Belogianni *et al.* (WA91 Collaboration), Confirmation of a soft photon signal in excess of QED expectations in π^-p interactions at 280 GeV/c, Phys. Lett. B 408, 487 (1997).
5. A. Belogianni *et al.* (WA102 Collaboration), Observation of a soft photon signal in excess of QED expectations in pp interactions, Phys. Lett. B 548, 129 (2002).
6. J. Abdallah *et al.* (DELPHI Collaboration), Evidence for an excess of soft photons in hadronic decays of Z^0 , Eur. Phys. J. C 47, 273 (2006), arXiv:hep-ex/0604038.
7. J. Abdallah *et al.* (DELPHI Collaboration), Observation of the muon inner bremsstrahlung at LEP1, Eur. Phys. J. C 57, 499 (2008), arXiv:0901.4488.
8. V. Perepelitsa, for the DELPHI Collaboration, Anomalous soft photons in hadronic decays of Z^0 , Proceedings of the XXXIX International Symposium on Multiparticle Dynamics, Gomel, Belarus, September 4-9, 2009, Nonlin. Phenom. Complex Syst. 12, 343 (2009).
9. J. Abdallah *et al.* (DELPHI Collaboration), Study of the dependence of direct soft photon production on the jet characteristics in hadronic Z^0 decays, Eur. Phys. J. C 67, 343 (2010), arXiv:1004.1587.
10. A. J. Krasznahorkay *et al.*, Observation of anomalous internal pair creation in ^8Be : a possible indication of a light, neutral boson, Phys. Rev. Lett. 116, 042501 (2016), arXiv:1504.01527.
11. A. J. Krasznahorkay *et al.*, New evidence supporting the existence of the hypothetical X17 particle, arXiv:1910.10459 (2019).
12. P. L. Jain and G. Singh, Search for new particles decaying into electron pairs of mass below 100 MeV/c², Jour. Phys. Phys. G 34, 129 (2007).
13. K. Abraamyan, A. B. Anisimov, M. I. Baznat, K. K. Gudima, M. A. Nazarenko, S. G. Reznikov, and A.S. Sorin, Observation of the E(38)-boson, arXiv:1208.3829v1 (2012).
14. K. Abraamyan, C. Austin, M. Baznat, K. Gudima, M. Kozhin, S. Reznikov, and A. Sorin, Check of the structure in photon pairs spectra at the invariant mass of about 38 MeV/c², EPJ Web of Conferences 204, 08004 (2019).
15. E. van Beveren and G. Rupp, First indications of the existence of a 38 MeV light scalar boson, arXiv:1102.1863 (2011).
16. E. van Beveren and G. Rupp, Material evidence of a 38 MeV boson, arXiv:1202.1739 (2012).
17. L. Van Hove, Cold quark-gluon plasma and multiparticle production, Ann. Phys. (N.Y.) 192, 66 (1989).
18. P. Lichard and L. Van Hove, The cold quark-gluon plasma as a source of very soft photons in high energy collisions, Phys. Lett. B 245, 605 (1990).
19. V. Balek, N. Pisutova, and J. Pisut, The puzzle of very soft photon production in hadronic Interactions, Acta Phys. Pol. B 21, 149 (1990).
20. S.M. Darbinian, K.A. Ispirian, A.T. Margarian, Unruh radiation of quarks and the soft photon puzzle in hadronic interactions, Sov. J. Nucl. Phys. 54, 364 (1991).
21. W. Czyz and W. Florkowski, Soft photon production in the boost invariant color flux tube model, Z. Phys. C 61, 171 (1994).
22. P. Lichard, Consistency of data on soft photon production in hadronic interactions, Phys. Rev. D 50, 6824 (1994).
23. O. Nachtmann, Nonperturbative QCD effects in high-energy collisions, hep-ph/9411345.
24. G.W. Botz, P. Haberl, O. Nachtmann, Soft photons in hadron-hadron collisions: Synchrotron radiation from the QCD vacuum?, Z. Phys. C 67, 143 (1995).
25. E. Kokoulina, A. Kutov, V. Nikitin, Braz. J. Phys., 37, 785 (2007);.
26. M. Volkov, E. Kokoulina, E. Kuraev, Gluon dominance model and cluster production, Ukr. J. Phys., 49, 1252 (2003).
27. Yoshitaka Hatta and Takahiro Ueda, Soft photon anomaly and gauge/string duality, Nucl. Phys. B 837, 22 (2010), [arXiv:1002.3452].
28. C. Y. Wong, Anomalous soft photons in hadron production, Phys. Rev. C 81, 064903 (2010), [arXiv:1001.1691].
29. C. Y. Wong, Anomalous soft photons associated with hadron production in string fragmentation, Talk presented at the IX International Conference on Quark Confinement and Hadron Spectrum, Madrid, Spain, Aug 30-Sept 3, 2010, AIP Conf. Proc. 1343:447 (2011), [arXiv:1011.6265].
30. C. Y. Wong, An overview of the anomalous soft photons in hadron production, Talk presented at International Conference on the Structure and the Interactions of the Photon, 20-24 May 2013, Paris, France, [arXiv:1404.0040].
31. C. Y. Wong, Open string QED meson description of the X17 particle and dark matter, JHEP 08 (2020) 165, [arXiv:2001.04864].
32. C. Y. Wong, QED mesons, the QED neutron, and the dark matter, EPJ Web Conf. 259, 13016 (2022), [arXiv:2108.00959].
33. C. Y. Wong, QED meson description of the x17 and other anomalous particles, Talk presented at Workshop on "Shedding Light on X17", September 6-8, 2021, Centro Ricerche Enrico Fermi, Rome, Italy; Editors M. Raggi *et al.*, [arXiv: arXiv:2201.09764].
34. A. V. Koshelkin, C. Y. Wong, Dynamics of quarks and gauge fields in the lowest-energy states in QCD and QED, arXiv:2111.14933 (to be published).
35. D. E. Kharzeev, F. Loshaj, Anomalous soft photon production from the induced currents in Dirac sea, Phys. Rev. D 89, 074053 (2014).
36. Xilin Zhang, G. A. Miller, Can nuclear physics explain the anomaly observed in the internal pair production in the Beryllium-8 nucleus?, Phys. Lett. B 773, 159 (2017), [arXiv:1703.04588].
37. J. Feng *et al.*, Protophobic fifth force interpretation of the observed anomaly in ^8Be nuclear transitions, Phys. Rev. Lett. 2016 117, 071803 (2016).
38. J. Feng *et al.*, Particle physics models for the 17 MeV anomaly in beryllium nuclear decays, Phys. Rev. D 95, 035017 (2017).

39. B. Fornal, Is there a sign of new physics in beryllium transitions ?, *Int. J. Mod. Phys. A* 32, 1730020 (2017).
40. Jose Bordes, Chan Hong-Mo, Tsou Sheung Tsun, Accommodating three low-scale anomalies ($g-2$, Lamb shift, and Atomki) in the framed standard model , *Int.J.Mod.Phys.A* 34 (2019) 25, 1830034 (2019) and references cited therein.
41. J. Batley *et al.* (NA48/2 Collaboration), Search for the dark photon in π^0 decays, *Phys. Lett. B* 746, 178 (2015), [arXiv:1504.00607].
42. Luigi Delle Rose *et al.*, Explanation of the 17 MeV Atomki anomaly in a $U(1)$ -extended two Higgs doublet model, *Phys. Rev. D* 96, 115024 (2017).
43. Lugi Delle Rose *et al.*, Atomki anomaly in family-dependent $U(1)$ extension of the standard model , *Phys. Rev. D* 99 055022 (2019).
44. Lugi Delle Rose *et al.*, New physics suggested by Atomki anomaly , *Frontiers in Physics* 7 73 (2019).
45. U. Ellwanger and S. Moretti, Possible explanation of the electron positron anomaly at 17 MeV in ^8Be transitions through a light pseudoscalar , *JHEP* 11 39 (2016).
46. D.S.M. Alves, and N. J. Weiner, A viable QCD axion in the MeV mass range , *JHEP* 07 92, (2018).
47. M. Munch *et al.*, Measurement of the full excitation spectrum of the $^7\text{Li}(p, \gamma)\alpha\alpha$ reaction at 441 keV , *Phys. Lett. B* 782, 779 (2018), [arXiv:1802.10404].
48. D. Banerjee *et al.*, (NA64 Collaboration), Improved limits on a hypothetical $X(16.7)$ boson and a dark photon decaying into e^+e^- pairs, [arXiv:1912.11389] and references cited therein.
49. C. Taruggi, A. Ghoshal, and M. Raggi (for the PADME Collaboration), Searching for dark photons with the PADME experiment , (Conference: C18-05-07.4, p.17-21, p.28-34, and 337-344), *Frascati Phys. Ser.* 67, 17, 28, and 334 (2018).
50. C. Hati, J. Kriewald, J. Orloff, A.M. Teixeira, Anomalies in ^8Be nuclear transitions and $(g-2)_{e\mu}$, *JHEP* 07 (2020) 235, [arXiv:2005.00028].
51. O. Seto, T. Shimomura, Atomki anomaly in gauged $U(1)_R$ symmetric model , *JHEP* 04 (2021) 025, [arxiv:2006.05497].
52. A T D'yachenko and E S Gromova, Detection of particles of dark matter from the spectrum of secondary pp collisions , *Jour. Phys. Conf. Series*, 2131, 022054, (2021).
53. See Proceedings of Workshop on "Shedding Light on X17", September 6-8, 2021, Centro Ricerche Enrico Fermi, Rome, Italy; Editors: M. Raggi, P. Valente, M. Nardecchia, A. Frankenthal, G. Cavoto, and references cited therein.
54. J. Schwinger, Gauge invariance and mass II , *Phys. Rev.* 128, 2425 (1962).
55. J. Schwinger, Gauge theory of vector particles , in *Theoretical Physics, Trieste Lectures, 1962* (IAEA, Vienna, 1963), p. 89.
56. S. Coleman, R. Jackiw, and L. Susskind, Charge shielding and quark confinement in the massive Schwinger model , *Ann. Phys.* 93, 267 (1975).
57. S. Coleman, More about the massive Schwinger model , *Ann. Phys.* 101, 239 (1976).
58. M. B. Halpern, Quantum "solitons" which are $SU(N)$ fermions , *Phys. Rev. D* 12, 1684 (1975).
59. A. Casher, J. Kogut, and L. Susskind, Vacuum polarization and the absence of free quarks, *Phys. Rev. D* 10, 732 (1974).
60. E. Witten, Non-Abelian bosonisation in two dimensions , *Commun. Math. Phys.* 92, 455 (1984).
61. Y. Frishman and J. Sonnenschein, Bosonization and QCD in two dimensions , *Phys. Rep.* 223, 309 (1993).
62. C. Y. Wong, R. C. Wang, and J. S. Wu, Schwinger particle production mechanism for a finite length flux tube with transverse confinement , *Phys. Rev. D* 51, 3940 (1995).
63. Y. Hosotani and R. Ridgriguez, Bosonized massive N-avour Schwinger model , *J. Phys. A* 31, 9925 (1998).
64. E. Abdalla, M. C. B. Abdalla, and K. D. Rothe, *Two Dimensional quantum field theory* , World Scientific Publishing Company, Singapore, 2001.
65. S. Nagy, Massless fermions in multi flavor QED , *Phys. Rev. D* 79, 045004 (2009).
66. PDG2019, M. Tanabashi *et al.*, *Review of Particle Physics*, *Phys. Rev. D* 98, 030001 (2019).
67. D. F. Geesaman and P. E. Reimer, The sea of quarks and antiquarks in the nucleon , *Rep. Prog. Phys.*, 82, 252003 (2010)
68. Kyle D. Bednar, Ian C. Clot, and Peter C. Tandy, Distinguishing Quarks and Gluons in Pion and Kaon Parton Distribution Functions , *Phys. Rev. Lett.* 124, 042002 (2020)
69. A. V. Koshelkin, C. Y. Wong, The compactification of QCD4 to QCD2 in a flux tube , *Phys. Rev. D* 86, 125026 (2012), [arXiv:1212.3301].
70. G. Veneziano, Construction of a crossing-symmetric, Regge-behaved amplitude for linearly rising trajectories, *Nuovo Cim* 57A, 190 (1968).
71. Y. Nambu, Quark model of the factorization of the Veneziano Amplitude , in *Lectures at the Copenhagen Symposium: Symmetry and Quark Models* , edited by R. Chand, Gordon and Breach, 1970, p. 269.
72. T. Goto, Relativistic quantum mechanics of one-dimensional mechanical continuum and subsidiary condition of dual resonance model *Prog. Theo. Phys*, 46, 1560 (1971).
73. G. 't Hooft, A planar diagram theory for strong interactions, *Nucl. Phys.* B72, 461 (1974).
74. G. 't Hooft, A two-dimensional model for mesons , *Nucl. Phys.* B75, 461 (1974).
75. X. Artru, G. Mennessier, String model and multiproduction *Nucl. Phys.* B70, 93 (1974).
76. B. Andersson, G. Gustafson, and T. Sjöstrand, A General Model for Jet Fragmentation , *Zeit. für Phys.* C20, 317 (1983).
77. S. Huang, J. W. Negele, J. Polonyi, Meson structure in QCD2 . *Nucl. Phys. B* 307, 669 (1988).
78. G.S. Bali, H. Neff, T. Duessel, T. Lippert, K. Schilling (SESAM), Observing long colour flux tubes in $SU(2)$ lattice gauge theory , *Phys.Rev.D* 71,114513(2005), [arxiv:hep-lat/0505012].
79. L. Cosmai, P. Cea, F. Cuteri, A. Papa, Flux tubes in QCD with $(2+1)$ HISQ fermions , *Pos, 4th annual International Symposium on Lattice Field Theory 24-30 July 2016 University of Southampton, UK*, [arXiv:1701.03371].
80. A. M. Polyakov, Quark confinement and topology of gauge theories *Nucl. Phys.* B120, 429 (1977).
81. A. M. Polyakov, *Gauge fields and strings* , Hardwood Publishers, Switzerland, 1987.
82. S. D. Drell, H. R. Quinn, B. Svetitsky, and M. Weinstein, Quantum electrodynamics on a lattice: A Hamiltonian variational approach to the physics of the weak-coupling region, *Phys. Rev. D* 19, 619 (1979).
83. C. N. Yang, Charge quantization, compactness of the gauge group, and flux quantization , *Phys. Rev. D* 1, 2360 (1970).
84. C. Y. Wong, The Wigner function of produced particles in string fragmentation , *Phys. Rev. C* 80, 054917 (2009), [arXiv:0903.3879].

85. K. G. Wilson, Confinement of quarks, *Phys. Rev. D* 19, 2445 (1974).
86. G. 'tHooft, Magnetic monopoles in unified gauge theories, *Nucl. Phys. B* 79, 276 (1974).
87. J. Kogut and L. Susskind, Hamiltonian formulation of Wilson's lattice gauge theories, *Phys. Rev. D* 11, 395 (1975).
88. S. Mandelstam, Vortices and quark confinement in non-abelian gauge theories, *Phys. Lett.* 53B, 476 (1975).
89. T. Banks, B. Myerson, and J. Kogut, Phase transitions in Abelian lattice gauge theories, *Nucl. Phys. B* 129, 493 (1977).
90. J. Glimm and A. Jaffe, Instantons in a $U(1)$ lattice gauge theory: A Coulomb dipole gas, *Comm. Math. Phys.* 56, 195 (1977).
91. M. E. Peskin, Mandelstam-'t Hooft duality in Abelian lattice models, *Ann. Phys. (N. Y.)* 113, 122 (1978).
92. A. Guth, Existence proof of a nonconfining phase in four-dimensional $U(1)$ lattice gauge theory, *Phys. Rev. D* 21, 2291 (1980).
93. K-I Kondo, Existence of confinement phase in quantum electrodynamics, *Phys. Rev. D* 58, 085013 (1998).
94. G. Magnifico, T. Felsner, P. Silvi, S. Montangero, Lattice quantum electrodynamics in (3+1)-dimensions at finite density with tensor networks, *Nature Comm.* 12, 3600 (2021), [arXiv:2011.10658].
95. J. Bender and E. Zohar, A gauge redundancy-free formulation of compact QED with dynamical matter for quantum and classical computations, *Phys. Rev. D* 102, 114517 (2020), [arXiv:2008.01349].
96. C. W. Bauer, D. M. Grabowska, Efficient representation for simulating $u(1)$ gauge theories on digital quantum computers at all values of the coupling, [arXiv:2111.08015].
97. D. B. Kaplan and J. R. Stryker Gauss's law, duality, and the Hamiltonian formulation of $U(1)$ lattice gauge theory *Phys. Rev. D* 102, 094515 (2020),
98. C. Y. Wong, Introduction to high-energy heavy-ion collisions, (World Scientific, Singapore, 1994).
99. H. Georgi, The Schwinger point, *JHEP* 11 (2019) 057, [arXiv:1905.09632].
100. H. Georgi and B. Noether, Non-perturbative Effects and Unparticle Physics in Generalized Schwinger Models, [arXiv:1908.03279v3].
101. H. Georgi and B. Warner, Generalizations of the Sommerfeld and Schwinger models, *JHEP* 01, 047 (2020), [arXiv:1907.12705v2].
102. P. A. M. Dirac, Lectures on Quantum Mechanics, Yeshiva University, New York, 1964.
103. I. T. Todorov, Quasipotential Equation Corresponding to the Relativistic Eikonal Approximation, *Phys. Rev. D* 3, 2351 (1971).
104. H. W. Crater and P. Van Alstine, Two-body Dirac equations, *Ann. Phys. (N.Y.)*, 148, 57 (1983).
105. H. W. Crater, R. L. Becker, C. Y. Wong, and P. Van Alstine, Nonperturbative solution of two-body Dirac equations for quantum electrodynamics and related field theories, *Phys. Rev. D* 46, 5117 (1992).
106. H. Crater, C. Y. Wong, P. Van Alstine, Tests of two-body Dirac equation wave functions in the decays of quarkonium and positronium into two photons, *Phys. Rev. D* 74, 054028 (2006), [arxiv:hep-ph/0603126].
107. H. W. Crater, C. Y. Wong, Two gamma quarkonium and positronium decays with Two-Body Dirac equations of constraint dynamics, *J. Phys. Conf. Ser.* 69, 012021 (2007), [arxiv:hep-ph/0701045].
108. H. W. Crater, Jin-Hee Yoon and C. Y. Wong, Singularity Structures in Coulomb-Type Potentials in Two Body Dirac Equations of Constraint Dynamics, *Phys. Rev. D* 79, 034011 (2009), [arXiv:0811.0732].
109. H. W. Crater and James Schiermeyer, Applications of two-body Dirac equations to the meson spectrum, *Phys. Rev. D* 82, 094020 (2010), [arXiv:1004.2980].
110. C. Y. Wong, H. W. Crater, The Relativistic N-body Problem in a Separable Two-Body Basis, *Phys. Rev. C* 63, 044907 (2001), [arXiv:nucl-th/0010003].
111. H. Sazdjian, The connection of two-particle relativistic quantum mechanics with the Bethe-Salpeter equation, *J. Math. Phys.* 28 2618 (1987)
112. H. Sazdjian, N-body bound state relativistic wave equations, *Ann. of Phys.* 191, 52(1989).
113. C. Y. Wong, On the Schrödinger equation in uid-dynamical form, *J. Math. Phys.* 17, 1008 (1976).
114. E. Annala, T. Gorda, A. Kurkela, J. Naettilae, and A. Vuorinen, Evidence for quark-matter cores in massive neutron stars, *Nat. Phys.* 16, 907 (2020)
115. R. Essig, The Low-Mass Dark Matter Frontier, *Physics*, 13, 172 (2020) and references cited therein.
116. D. L. Hill and J. A. Wheeler, Nuclear Constitution and the Interpretation of Fission Phenomena, *Phys. Rev.* 89, 1102 (1953).
117. M. Brack, J. Damgaard, A. S. Jensen, H. C. Pauli, V. M. Strutinsky, and C. Y. Wong, Funny Hills: The Shell-Correction Approach to Nuclear Shell Effects and Its Applications to the Fission Process, *Rev. Mod. Phys.* 44, 320 (1972).
118. B. P. Abbott *et al.* (LIGO Collaboration), GW170817: Observation of Gravitational Waves from a Binary Neutron Star Inspiral, *Phys. Rev. Lett.* 119, 161101 (2017).
119. A. Bauswein, N-U. F. Bastian, D. Blaschke, K. Chatzizoannou, J. A. Clark, T. Fischer, and M. Oertel, Identifying a first-order phase transition in neutron-star mergers through gravitational waves, *Phys. Rev. Lett.* 122, 061102 (2019).
120. A. Bauswein, S. Blacker, V. Vijayan, N. Stergioulas, K. Chatzizoannou, J. A. Clark, N-U F. Bastian, D. B. Blaschke, M. Cierniak, and T. Fischer, Equation of state constraints from the threshold binary mass for prompt collapse of neutron star mergers, *Phys. Rev. Lett.* 125, 141103 (2020).
121. L. R. Weih, M. Hanauske, and L. Rezzolla, Postmerger gravitational-wave signatures of phase transitions in binary mergers, *Phys. Rev. Lett.* 124, 171103 (2020).
122. A. De Rújula, H. Georgi, and S. L. Glashow, Hadron masses in a gauge theory, *Phys. Rev. D* 12, 147 (1975).
123. S. Godfrey and N. Isgur, Mesons in a relativized quark model with chromodynamics, *Phys. Rev. D* 132, 189 (1985).
124. T. Barnes and E. S. Swanson, Diagrammatic approach to meson-meson scattering in the nonrelativistic quark potential model, *Phys. Rev. D* 46, 131 (1992).
125. C. Y. Wong, E. S. Swanson, T. Barnes, Cross Sections for pi- and rho-induced Dissociation of J/ψ and ψ' , *Phys. Rev. C* 62, 045201 (2000), [arXiv:hep-ph/9912431]
126. C. Y. Wong, E. S. Swanson, and T. Barnes, Heavy quarkonium dissociation cross sections in relativistic heavy-ion collisions, *Phys. Rev. C* 65, 014903 (2001), [arXiv:nucl-th/0106067].
127. L. D. Landau, The moment of a 2-photon system, *Dokl. Akad. Nauk SSSR.* 60, 207 (1948).
128. C. N. Yang, Selection rules for the dematerialization of a particle into two photons, *Phys. Rev.* 77, 242-245 (1950).